

# DocDjinn: Controllable Synthetic Document Generation with VLMs and Handwriting Diffusion

Marcel Lamott<sup>\*1</sup>, Saifullah Saifullah<sup>\*2,3</sup>, Nauman Riaz<sup>\*2,3</sup>, Yves-Noel Weweler<sup>4</sup>, Tobias Alt-Veit<sup>4</sup>, Ahmad Sarmad Ali<sup>5</sup>, Muhammad Armaghan Shakir<sup>5</sup>, Adrian Kalwa<sup>1</sup>, Momina Moetesum<sup>5</sup>, Andreas Dengel<sup>2</sup>, Sheraz Ahmed<sup>2,3</sup>, Faisal Shafait<sup>5</sup>, Ulrich Schwanecke<sup>1</sup>, and Adrian Ulges<sup>1</sup>

<sup>1</sup> RheinMain University of Applied Sciences, Wiesbaden, Germany

<sup>2</sup> German Research Center for Artificial Intelligence, Kaiserslautern, Germany

<sup>3</sup> DeepReader GmbH, Kaiserslautern, Germany

<sup>4</sup> Insiders Technologies GmbH, Kaiserslautern, Germany

<sup>5</sup> National University of Sciences and Technology (NUST), Islamabad, Pakistan

**Abstract.** Effective document intelligence models rely on large amounts of annotated training data. However, procuring sufficient and high-quality data poses significant challenges due to the labor-intensive and costly nature of data acquisition. Additionally, leveraging language models to annotate real documents raises concerns about data privacy. Synthetic document generation has emerged as a promising, privacy-preserving alternative. We propose DocDjinn, a novel framework for controllable synthetic document generation using Vision-Language Models (VLMs) that produces annotated documents from unlabeled seed samples. Our approach generates visually plausible and semantically consistent synthetic documents that follow the distribution of an existing source dataset through clustering-based seed selection with parametrized sampling. By enriching documents with realistic diffusion-based handwriting and contextual visual elements via semantic-visual decoupling, we generate diverse, high-quality annotated synthetic documents. We evaluate across eleven benchmarks spanning key information extraction, question answering, document classification, and document layout analysis. To our knowledge, this is the first work demonstrating that VLMs can generate faithful annotated document datasets at scale from unlabeled seeds that can effectively enrich or approximate real, manually annotated data for diverse document understanding tasks. We show that with only 100 real training samples, our framework achieves on average 87% of the performance of the full real-world dataset. We publicly release our code and 140k+ synthetic document samples.

**Keywords:** Document synthesis · Synthetic data generation · Vision-Language Models · Handwriting diffusion · Document understanding · Seed selection

---

\* Equal contribution.

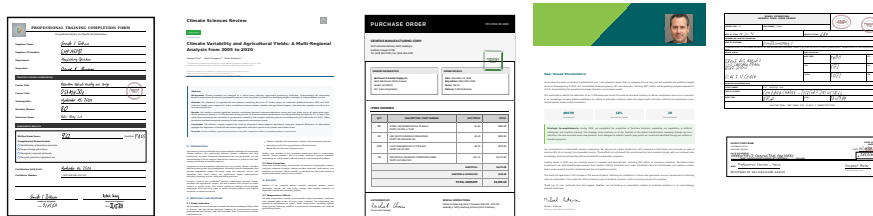


Fig. 1: Examples of synthetically generated documents across diverse domains and tasks. Our framework produces documents with realistic layouts, VLM-generated content, diffusion-based handwriting, and contextual visual elements.

## 1 Introduction

Document intelligence systems employ deep learning and Vision-Language Models (VLMs) to transform documents into structured information via document layout analysis (DLA) [60], key information extraction (KIE) [26], visual question answering (VQA) [38], and classification (CLS). While VLMs are powerful, they remain prohibitively expensive for specialized, high-throughput applications. This has motivated smaller, task-specific models [4] that require substantial labeled training data. Despite recent datasets [57,17], obtaining high-quality annotations for diverse document types remains costly and labor-intensive.

Synthetic data generation offers a promising solution. However, existing approaches either lack textual coherence [56], generate only task-specific content such as layout [23] or tables [20], or produce documents without ground truth (GT) annotations [8,33,14,1]. DocGenie [21], while capable of conditioning generation on seed documents, generates only visual content and text without task-specific labels required for supervised learning (*e.g.* entity labels for KIE, bounding boxes for DLA, question-answer pairs for VQA). Consequently, these synthetic documents cannot directly train document understanding models.

We present DocDjinn, addressing three key challenges: **(1) Multimodal realism** through VLM-generated content combined with diffusion-based handwriting synthesis and contextual visual element insertion, **(2) distribution alignment** via automatic clustering-based seed selection with parametrized sampling strategies that align synthetic data with source dataset distributions, and **(3) training suitability** by generating high-quality task-specific annotations alongside documents, enabling direct supervised learning across VQA, KIE, CLS, and DLA tasks.

Our evaluation demonstrates that synthetic-only training achieves 70.8% of real-data performance, while augmenting just 100 real samples with synthetic data reaches within 9.45 points of full real-data training. In low-resource scenarios with only 100 labeled samples, our framework achieves on average 87% of the performance of the full real-world dataset.

Our concrete contributions are as follows:

Table 1: Overview of recent synthetic document generation approaches compared to ours. **Target** specifies the generated modality, and **Source** the conditioning input. **Text**, **HW**, and **VE** indicate explicit support for readable text, readable handwritten text, and visual elements during generation. **U. GT.** represents the capability to automatically generate task annotations in an unsupervised manner. **Max Res.** denotes the maximum possible generation resolution, whereas **Dyn. Spec.** represents whether the generation process can be controlled via natural language. **ML** indicates multilingual generation ability, and **OS** indicates whether the framework is open source. Finally, **Editable** indicates whether generated documents are produced in an editable format (e.g., structured text) rather than as rasterized images.

Year Name	Model	Target	Source	Text	HW	VE	U. GT.	Tasks	Max Res.	Dyn. Spec.	ML	OS	Editable
2017 DocCreator [31]	manual	full document	images	✓	✗	✗	✓	OCR / DLA	-	✗	✓	✓	✗
2019 Bui et al. [8]	GAN	document image	text	✓	✗	✗	✗	OCR	512 × 512	✗	✗	✗	✗
2021 Genalog [19]	templates	document image	text	✓	✗	✗	✗	NER	Unspec.	✗	✗	✓	✗
2021 DocSynth [5]	GAN	document image	layout	✗	✗	✓	✗	✗	128 × 128	✗	✗	✓	✓
2021 Raman et al. [47]	sampling	full document	layout	✓	✗	✓	✓	DLA	Unspec.	✗	✓	✗	✗
2022 SynthDoG [33]	sampling	full document	-	✓	✗	✗	✓	DLA	2560 × 1920	✗	✓	✓	✗
2023 Tanveer et al. [56]	DPM	document image	layout	✗	✗	✓	✗	DLA	256 × 256	✗	✗	✗	✓
2023 DocGen [2]	LLM	document text	text	✓	✗	✗	✗	IR	-	✓	✗	✓	✓
2023 Fennir et al. [15]	GAN	document image	layout	✗	✗	✗	✗	✗	512 × 512	✗	✗	✗	✓
2024 Hamdani et al. [20]	DPM	table image	layout	✗	✗	✗	✗	TE	512 × 512	✗	✗	✗	✗
2024 SynthDoc [14]	sampling	full document	text	✓	✗	✓	✓	KIE	1280 × 960	✗	✓	✗	✓
2024 Hou et al. [27]	sampling	full table	text+layout	✓	✗	✗	✗	TE	-	✗	✓	✗	✓
2025 Havas [1]	LLM	full document	template	✓	✗	✗	✓	KIE	-	✓	✓	✗	✓
2025 DocGenie [21]	VLM	full document	images	✓	✗	✗	✗	✗	-	✓	✓	✗	✓
2025 DocDjinn (Ours)	VLM	full document	images	✓	✓	✓	✓	CLS / KIE / VQA / DLA	-	✓	✓	✓	✓

- A scalable framework for synthetic document generation that produces automatic ground truth annotations from unlabeled seed documents across VQA, KIE, CLS, and DLA tasks.
- First integration of diffusion-generated handwriting into modern document synthesis with semantic-visual decoupling for stamps, barcodes, and logos.
- Clustering-based seed selection with parametrized sampling that preserves target distributions.
- Public release of eleven synthetic datasets (140k+ samples) and DocVQA-HW, a handwriting-focused DocVQA [38] subset.

## 2 Related Work

Recent document intelligence models mainly rely on transformers [58,28] and LLMs [13,7,46]. While specialized models exist for sub-tasks such as table analysis [40] or key information extraction [26], recent models aim at multi-task full document understanding [58,33,28,58]. Curating high-quality datasets from real-world documents is challenging if not infeasible, if these models need to be adapted to new domains or trained from scratch. Thus, researchers have turned towards synthetic training data [3], fostering a plethora of synthetic document generation frameworks in recent years [21,5,33]. We list a selection thereof in Tab. 1. These works can be grouped mainly along two dimensions: the underlying model architecture, and the targeted modality of generated data. In addition,

we highlight the differences between approaches in terms of the input source, support for text (printed/handwritten) and visual elements, maximum possible generation resolution, controllability via natural language, multilingual support, and whether the documents can be easily edited post-generation.

Barring exceptions, four classes of models emerge: sampling-based strategies [14,33,27], Generative Adversarial Networks (GANs) [8,5,15], diffusion probabilistic models (DPMs) [54], and Large Language Models (LLMs) [13,46]. Both GANs and DPMs excel at visual synthesis, enabling specialized applications in document image generation [56,20], document layout generation [23,35], and handwritten text generation [41,50,12]. However, they inherently lack the ability to generate coherent, contextually grounded text at large scale, as it requires discrete sequential modeling and linguistic reasoning capabilities beyond their visual architectures.

In contrast, the language generation capabilities of LLMs [13,46] represent a significant advancement, allowing for controllable synthetic generation of full documents. While LLMs lack the visual generation qualities of diffusion models to synthesize specialized visual content, such as realistic handwritten text with consistent style and natural variations, their recent extension to VLMs [45,59] enables them to reliably process visual data. As they have been trained on markup languages, among other data, they are capable of producing visual elements solely based on markup. This is sufficient for satisfactory synthetic document generation, as the majority of documents share a structured layout. Unsurprisingly, the state of the art in synthetic document generation employs LLMs and VLMs [1,21].

Out of all recent works, to the best of our knowledge, only six works fulfill the requirements of full document generation [31,33,14,1,21,47]. Among these, DocCreator [31], SynthDoG [33], SynthDoc [14], and Raman et al. [47] all rely on predefined templates or sampling from public corpora that limit their applications in specialized domains. Abarca & Havas [1] generate full documents with LLMs but rely on manually crafted dataset-specific templates, limiting the generalization of their approach. DocGenie [21] is the only approach that can leverage documents directly as a dynamic source without having to extract a specific modality from the source data or rely on handcrafted templates. However, since it does not produce task-specific ground-truth annotations, its applicability in downstream applications is limited. In addition, DocGenie [21] randomly selects seed samples from the source distribution to generate new documents. This limits the scalability of the approach for large document corpora, which often exhibit substantial class imbalance and contain large clusters of highly similar documents within the data distribution.

We improve upon the limitations of DocGenie [21] by automating seed selection to obtain a representative set that captures the source data distribution and by enabling the VLM to generate task-specific ground-truth annotations. Furthermore, we combine the advantages of VLMs with those of DPMs by generating visual annotations with the VLM that serve as conditioning input for a DPM. The DPM then generates variable-style realistic handwritten text, which

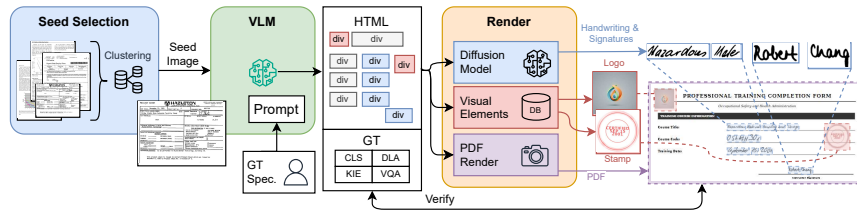


Fig. 2: Overview of DocDjinn for synthetic document generation. After selecting representative seeds from a source dataset, a VLM generates an HTML representation of the document, along with multi-task ground truth information. This representation is enhanced with diffusion-generated handwriting and further visual elements. Finally, the ground truth is updated with bounding boxes and verified.

is injected into the documents. Thus, we present a fully automatic and unsupervised pipeline to enrich real-world datasets with plausible synthetic samples that can be directly used in downstream tasks.

### 3 Our Framework: DocDjinn

We propose *DocDjinn*, a VLM-based framework for generating synthetic documents with realistic content and structurally coherent layouts alongside task-specific ground-truth annotations. Assuming a set of real unlabeled documents  $\mathcal{D}_{\text{real}} = \{x_i\}_{i=1}^N$ , we seek to substitute or complement it with a synthetic dataset  $\mathcal{D}_{\text{syn}} = \{(x'_i, y'_i)\}_{i=1}^{N'}$  such that a model trained on the synthetic dataset, either alone or in combination with the real dataset, approximates the original model performance on a given task. Here,  $x'_i$  denotes a synthetically generated document sample, and  $y'_i$  its corresponding annotation. DocDjinn operates in four stages, an overview of which is given in Fig. 2: (1) intelligent seed sample selection, (2) seed-guided VLM-based document and GT synthesis, (3) visual realism enhancement via insertion of diffusion-based handwriting and visual elements, and (4) bounding box extraction and GT verification.

#### 3.1 Intelligent Seed Sample Selection

Unlike previous work [21], where seed samples are randomly sampled from the source dataset, we introduce a clustering-based approach to select representative yet diverse seed samples. Seed-samples are document images supplied as few-shot examples to guide the VLM during the synthesis and condition it to produce similar documents.

*Embeddings.* To capture both the structural and semantic characteristics of each document, we first represent documents using embeddings derived from layout,

image, and text modalities. For each document  $d_i \in \mathcal{D}_{\text{real}}$ , we compute embeddings using LayoutLMv3 [28] CLS tokens (`layoutlm`), CLIP [45] image features (`clip`), and Sentence Transformers [48] text representations (`sentence`). We propose a multimodal embedding (`combined`) by z-score normalizing and concatenating these three modalities, capturing layout structure, visual appearance, and textual semantics jointly. We additionally compare against pooled LayoutLMv3 embeddings (`pooled`) [53].

*Clustering.* We adopt the approach from [53] by combining HDBSCAN with minimum cluster size  $\kappa$  and  $k$ -NN [16] with a fixed  $k$ . For each embedding type  $\mathcal{E}$  and minimum cluster size  $\kappa$ , embeddings  $\{\mathbf{e}_i\}_{i=1}^N$  are reduced to  $d'$  dimensions via UMAP. HDBSCAN produces initial clusters with noise points, which are then reassigned using a  $k$ -NN classifier trained on non-noise embeddings, ensuring complete coverage. We manually select the optimal clustering, assisted by a heuristic combining silhouette score and normalized entropy that empirically correlates well with clustering quality and favors high internal coherence and balanced cluster sizes (Appendix C).

*Sampling.* From  $K$  clusters with sizes  $\{n_c\}_{c=1}^K$ , we sample clusters with probabilities  $p(c) \propto n_c^\alpha$ , where  $\alpha$  controls cluster size bias. We compare two strategies for generations, in each of which  $n$  seeds are supplied as few-shot examples: *cross-cluster* (CC) samples  $n$  seeds independently (each according to  $p(c)$ ), while *intra-cluster* (IC) first samples one cluster via  $p(c)$ , then draws all  $n$  seeds from within that cluster. The resulting seed samples, consisting only of document images, are used to guide the VLM during document synthesis.

### 3.2 VLM-Based Document and GT Synthesis

Using the selected seed samples and a task-level prompt, we employ a VLM to synthesize HTML documents along with corresponding GT, generating  $M$  documents per prompt call while supplying  $2M$  seed images as guidance (compared to 10 seed images used in [21]). We distinguish two types of GT generation, corresponding to two prompt templates (see Appendix G): *Macro* (document-level JSON annotations), where the VLM is instructed to produce GT for VQA and simple KIE tasks, and *Micro* (element-level annotations with class labels), where labels are generated for layout- and structure-sensitive tasks, namely DLA and complex KIE. Each dataset is further defined by three parameters in the prompt template: **document type**, a brief description; **GT type**, specifying the annotation task (QA pair creation, KIE class labeling, document classification, or region-level labeling); and **GT format**, defining the ground-truth structure, *i.e.*, JSON or additional class groupings. We extract element regions from the HTML via JavaScript and match them to the generated GT for tasks requiring spatial annotations (KIE, DLA). Additionally, we extract bounding boxes from a PDF rendering of the HTML for subsequent processing steps.



Fig. 3: Baseline alignment for sentence-level handwritten text. **Top, left to right:** input image, word segmentation, lowest-ink pixel per column (in red), and computed baseline via percentile (in blue). **Bottom:** example sentence-level handwritten text after baseline alignment (red).

### 3.3 Visual Realism Enhancement

To improve realism, we add diffusion-based handwritten text and contextual visual elements such as figures and stamps to the documents, enhancing fidelity and bridging the domain gap to real documents. The VLM is prompted to produce HTML placeholders for such elements.

*Region Identification.* The VLM identifies regions requiring handwriting such as signatures or form fields, as well as visual elements (stamps, barcodes, logos, figures, and photos). For handwriting, it assigns author identifiers for multi-author generation. Each designated text element is rendered with a fixed font size, its region and word-level boxes are extracted, and the placeholders are replaced by diffusion-generated handwriting while preserving layout and semantics. Visual elements are typed and given textual content descriptions, such as “APPROVED 2024-03-15” for a stamp. Each visual element is rendered type-specific (details in Appendix E) and inserted into its corresponding region.

*Diffusion-based Handwriting.* To synthesize realistic handwritten text, we adopt a latent diffusion model [51,36,41,50] conditioned on both the target text and writer style. A pretrained Variational Autoencoder (VAE) is first used to encode the handwritten text images into latent variables  $z \in \mathbb{R}^{d_z}$ . Then, a conditional UNet-based diffusion model is trained in the latent space using the standard DPM loss [25]:

$$\mathcal{L}_{\text{DPM}}(\theta) = \mathbb{E}_{t, z_0, \epsilon} \left[ \left\| \epsilon - \epsilon_{\theta}(z_t, t; c_{\text{text}}, c_{\text{style}}) \right\|_2^2 \right], \quad (1)$$

where  $c_{\text{text}}$  denotes the text condition embedding obtained from a Transformer-based encoder model, and  $c_{\text{style}}$  represents the writer-specific style embedding (writer class). Details of our diffusion training and inference parameters are provided in Appendix D.

*Line-Segment Generation and Integration.* Handwritten text lines are generated by concatenating style-conditioned word segments from our diffusion model with baseline alignment (Fig. 3), where the baseline is the median y-coordinate of lowest ink pixels. After horizontal concatenation, segments are refined with Gaussian

blur, scaled to match their bounding box union, and positioned at their corresponding region location with random jitter (details in Appendix D). A manual inspection of 200 generated handwritten sentences shows that baseline alignment is correct in 89% of cases and remains acceptable in 84% under stricter visual assessment.

### 3.4 Bounding Box Extraction and GT Verification

Following visual enhancement, we extract text bounding boxes via Optical Character Recognition (OCR) for documents with handwritten/visual elements or PDF rendering for typeset documents. VLM-generated GT is verified using task-specific constraints: For VQA, answers must appear in text, verified using averaged normalized Levenshtein distance (ANLS [6]). For CLS, class labels need to be valid. In DLA, labels must be valid and regions within extracted bounds. For KIE, key-values need to appear in text, and region annotations constrained to designated areas. Documents failing verification or rendering to multiple pages are excluded.

## 4 Experiments

We evaluate DocDjinn along three axes: (i) its ability to generate visually and semantically faithful synthetic documents, (ii) the utility of these documents for downstream model training, and (iii) the impact of mixing synthetic and real-world data on model generalization. The experiments cover four major document understanding tasks: key information extraction (KIE), visual question answering (VQA), document classification (CLS), and document layout analysis (DLA).

### 4.1 Experimental Setup

*Embeddings and Clustering.* For embeddings, we use LayoutLMv3 [28] (`layout`), CLIP [45] (`clip`), and Sentence Transformers [48] (`sentence`). For `pooled` [53] LayoutLMv3 embeddings we use a kernel size of 4. Embeddings are projected to  $d' = 100$  via UMAP [39] before two-stage clustering, where we evaluate different min cluster sizes  $\kappa$  for HDBSCAN [10] and set  $k = 5$  for  $k$ -NN [16]. We select the embedding and  $\kappa$  for each dataset for downstream experiments according to Sec. 3.1, see Appendix C for details and dataset-specific clustering choices shown in Sec. C.

*Document Synthesis.* As VLM we use Claude Sonnet 4.5, as we deemed it the most capable VLM available for this task. We generate  $M = 3$  documents per prompt call for VQA, KIE, and CLS tasks, and  $M = 2$  for DLA tasks due to their more complex annotation requirements. VLM-generated HTML undergoes post-processing with JavaScript-based dimension measurement to ensure single-page PDF rendering via Playwright with dynamically computed page sizes. As text similarity threshold  $\text{ANLS}_\tau$  we use 75%.

*Handwriting Synthesis.* We employ a conditional latent diffusion model trained on IAM [37], using a pretrained VAE to encode each canonical  $128 \times 512$  word image into a  $16 \times 64$  latent ( $8 \times$  downsampling) while preserving stroke scale. Conditioning is applied on both text and writer identity via a UNet denoiser and Transformer text encoder. Using Microsoft Document Intelligence OCR<sup>1</sup> and visual inspection, we retain the top nine writers (CER/WER: 0.092/0.249 vs. 0.193/0.404), enabling legible multi-writer synthesis across documents. See Appendix D for training and architecture details.

*Datasets.* We conduct experiments on eleven datasets spanning multiple document understanding tasks: **VQA:** DocVQA [38] and WTQ [43]; **KIE:** KLC [55]<sup>2</sup>, SROIE [29], CORD [42], and FUNSD [30]; **CLS:** Tobacco3482 [34], RVL-CDIP [22], and DocLayNet-CLS [44]; **DLA:** PubLayNet [60], ICDAR2019 [18], and DocLayNet-DLA [44]. To manage costs while maintaining sufficient data volume, we limit training sets to 4,000 samples (except DocVQA, where we use the full train set to assess large-scale augmentation). This constraint reflects realistic resource limitations common in real-world applications. Details on dataset splits are given in Appendix B. We generate 1,000–10,000 synthetic samples per dataset at sampling rates  $\alpha \in \{0.5, 0.75, 1.0\}$ , totaling over 140k samples across all datasets (see Tabs. 9 and 10 in the appendix).<sup>3</sup> Additionally, we introduce DocVQA-HW, a 103-sample subset of DocVQA test split with handwritten content questions, to evaluate handwriting synthesis quality.<sup>4</sup>

*Models and Tasks.* We benchmark a diverse set of models representing major architectures for document understanding. We consider document understanding models BERT [13], LiLT [58], and LayoutLMv3 [28] for CLS, KIE, and VQA tasks, and pure vision baselines Faster R-CNN [49] and Cascade R-CNN [9] for DLA. Details to training hyperparameters are given in Appendix L.

*Metrics.* Performance is measured using task-appropriate metrics: ANLS for DocVQA, WTQ for WTQ [43], exact-match accuracy for CLS, F1-score for KIE, and mean Average Precision (mAP) for DLA. For generation quality, we employ FID [24] and Layout-FID [21] to assess distributional similarity between generated and real documents in pixel and learned feature spaces. We compute Layout-FID from LayoutLMv3 CLS-token embeddings. For PubLayNet and ICDAR2019, Layout-FID is computed from images only as text and bounding boxes are unavailable.

## 4.2 Seed Selection Strategies

We evaluate seed sampling strategies (Sec. 3.1) by training LayoutLMv3 (VQA, KIE, CLS) and Faster R-CNN (DLA) exclusively on synthetic data with cross-

<sup>1</sup> Model version 2024-11-30.

<sup>2</sup> KLC [55] is modeled as VQA for downstream evaluation (matching its extractive format) but generated as KIE during synthesis (see Sec. H).

<sup>3</sup> For code release and data availability, see Appendix M.

<sup>4</sup> For DocVQA-HW sample and question IDs, see Appendix M.

Dataset	Smpl	$\alpha = 0.50$		$\alpha = 0.75$		$\alpha = 1.00$	
		Score ( $\uparrow$ )	LFID ( $\downarrow$ )	Score ( $\uparrow$ )	LFID ( $\downarrow$ )	Score ( $\uparrow$ )	LFID ( $\downarrow$ )
DocVQA	CC	62.46	7.60	61.51	7.49	<b>63.16</b>	7.52
DocVQA	IC	63.95	6.88	<b>64.27</b>	6.87	63.64	6.96
CORD	CC	55.62	37.31	57.03	36.95	<b>57.74</b>	36.75
CORD	IC	57.51	36.92	56.56	37.01	<b>58.40</b>	36.46
RVL-CDIP	CC	43.65	11.15	45.49	12.45	<b>45.74</b>	11.06
RVL-CDIP	IC	51.90	8.62	51.04	9.88	<b>53.94</b>	8.82
PubLayNet	CC	61.99	3.53	<b>63.09</b>	2.75	61.00	2.81
PubLayNet	IC	63.06	2.63	<b>63.41</b>	2.63	62.90	2.50
<b>Average</b>	CC	55.93	14.90	56.78	14.91	<b>56.91</b>	<b>14.54</b>
<b>Average</b>	IC	59.11	13.76	58.82	14.10	<b>59.72</b>	<b>13.69</b>

Table 2: Layout-FID (LFID) [21] and performance comparison for CC and IC sampling across different  $\alpha$  values on LayoutLMv3 (VQA, KIE, CLS) and Faster R-CNN (DLA). Results averaged over 5 seeds (std < 0.04).

cluster (CC) versus intra-cluster (IC) sampling and varying  $\alpha \in \{0.50, 0.75, 1.00\}$ . Tab. 2 reports means over five random seeds (std < 0.04). Intra-cluster sampling consistently outperforms cross-cluster across all  $\alpha$  values (59.72% vs. 56.91% at  $\alpha = 1$ ), demonstrating that preserving structural coherence within document clusters is more critical than maximizing diversity across clusters. Within intra-cluster sampling,  $\alpha = 1$  achieves highest performance (59.72%) and lowest Layout-FID (13.69), indicating that biasing generation toward dominant document patterns produces superior synthetic data. The improvement is particularly pronounced for classification tasks, where IC outperforms CC by 8.2 points on RVL-CDIP at  $\alpha = 1$ . Based on these findings, we use intra-cluster sampling with  $\alpha = 1$  for all experiments.

### 4.3 Downstream Task Performance

We evaluate models on VQA, KIE, CLS, and DLA tasks under three data regimes: full-shot (Full), few-shot with 300 – 1000 real samples (Few<sub>A</sub>), and few-shot with 100 real samples (Few<sub>B</sub>). Results in Tab. 3 report means over three random seeds (std < 0.02).

Synthetic-only training demonstrates substantial quality. On DocVQA [38], real data outperforms pure synthetic by 5.05 points, but augmenting just 100 real samples reduces this gap to 3.93 points. On KLC [55], the gap is even smaller: real data exceeds pure synthetic by only 2.41 points, narrowing to 2.00 points with 100 real samples added. Performance gaps are larger on specialized datasets like CORD [42] (37–45 points) and DocLayNet-DLA [44] (39–43 points), reflecting domain-specific challenges in replicating real-world capture artifacts and complex annotations.

Combining real and synthetic data consistently matches or exceeds real-only performance, with improvements on DocVQA, WTQ, and ICDAR2019, averaging +0.51 points. Notably, vision-based LayoutLMv3 degrades on DocVQA-HW when adding synth data while text-only BERT improves, revealing that synthetic handwriting lacks authentic visual characteristics despite recognizable content, though the difficulty of this handwriting-focused subset makes isolated quality assessment challenging.

Model	Dataset	Task Metric (†)	Full			Few <sub>A</sub>		Few <sub>B</sub>		Δ		
			R	S	R+S	R	R+S	R	R+S	Full-Few <sub>B</sub>	R-S	
BERT	DocVQA	VQA	ANLS	57.97	52.92	61.33	46.63	55.45	25.61	54.04	3.93	5.05
LiLT	DocVQA	VQA	ANLS	70.50	64.34	72.53	58.99	66.95	38.59	64.11	6.39	6.16
LayoutLMv3	DocVQA	VQA	ANLS	71.45	66.03	<b>73.26</b>	62.91	<b>68.04</b>	43.61	<b>65.82</b>	5.63	5.42
BERT	DocVQA-HW	VQA	ANLS	48.24	42.26	51.19	40.94	44.07	26.47	42.72	5.51	5.97
LiLT	DocVQA-HW	VQA	ANLS	58.94	50.26	58.24	50.21	50.95	35.88	50.78	8.16	8.67
LayoutLMv3	DocVQA-HW	VQA	ANLS	<b>59.41</b>	51.25	58.36	52.31	<b>53.31</b>	41.20	<b>51.24</b>	8.17	8.16
BERT	WTQ	VQA	WTQ	16.51	9.24	19.39	15.68	18.50	6.65	13.84	2.68	7.27
LiLT	WTQ	VQA	WTQ	26.71	14.79	<b>30.90</b>	24.39	<b>29.50</b>	10.91	<b>22.46</b>	4.25	11.92
LayoutLMv3	WTQ	VQA	WTQ	25.64	12.76	29.47	24.20	28.66	7.86	21.61	4.04	12.89
Average VQA				48.37	40.43	50.52	41.81	46.16	26.31	42.96	<b>5.42</b>	<b>7.95</b>
BERT	CORD	KIE	F1	93.78	49.06	93.92	90.27	90.97	84.16	85.80	7.99	44.72
LiLT	CORD	KIE	F1	94.61	55.76	94.88	93.04	93.17	88.28	88.90	5.71	38.85
LayoutLMv3	CORD	KIE	F1	95.92	58.84	<b>96.56</b>	94.64	<b>95.13</b>	90.39	<b>92.05</b>	3.87	37.08
BERT	FUNSD	KIE	F1	56.33	40.84	59.19	-	-	54.18	56.46	-0.13	15.49
LiLT	FUNSD	KIE	F1	74.03	49.13	74.90	-	-	71.91	72.49	1.54	24.90
LayoutLMv3	FUNSD	KIE	F1	<b>88.56</b>	49.10	87.74	-	-	<b>87.46</b>	85.69	2.87	39.46
BERT	KLC	KIE	F1	45.22	41.90	45.00	43.98	44.46	33.66	43.11	2.11	3.32
LiLT	KLC	KIE	F1	46.08	43.66	<b>46.25</b>	45.07	45.32	37.44	<b>44.08</b>	2.00	2.41
LayoutLMv3	KLC	KIE	F1	46.11	43.24	46.11	<b>45.43</b>	45.22	37.84	43.64	2.47	2.86
BERT	SROIE	KIE	F1	88.12	60.94	88.97	83.78	85.32	74.90	79.35	8.77	27.18
LiLT	SROIE	KIE	F1	94.03	70.79	93.49	91.61	91.29	83.21	87.62	6.42	23.24
LayoutLMv3	SROIE	KIE	F1	94.17	72.32	<b>94.60</b>	91.05	<b>93.12</b>	83.82	<b>90.49</b>	3.68	21.85
Average KIE				76.41	52.97	76.80	75.43	76.00	68.94	72.47	<b>3.94</b>	<b>23.45</b>
BERT	DocLayNet-CLS	CLS	Acc	95.59	81.12	94.78	93.98	93.37	72.03	83.09	12.50	14.47
LiLT	DocLayNet-CLS	CLS	Acc	96.35	83.97	94.31	95.32	93.47	80.24	84.79	11.56	12.39
LayoutLMv3	DocLayNet-CLS	CLS	Acc	<b>97.33</b>	82.89	97.27	<b>96.33</b>	96.31	66.94	<b>89.90</b>	7.43	14.45
BERT	RVL-CDIP	CLS	Acc	76.87	44.40	75.23	70.06	67.65	33.48	55.42	21.45	32.46
LiLT	RVL-CDIP	CLS	Acc	78.78	48.72	77.68	72.41	69.43	41.16	57.99	20.79	30.06
LayoutLMv3	RVL-CDIP	CLS	Acc	<b>86.26</b>	53.84	85.64	<b>80.84</b>	80.29	19.68	<b>64.93</b>	21.33	32.42
BERT	Tobacco3482	CLS	Acc	86.05	59.62	84.57	81.48	79.86	36.91	63.52	22.53	26.43
LiLT	Tobacco3482	CLS	Acc	88.05	61.76	84.19	86.57	79.19	50.67	68.48	19.57	26.29
LayoutLMv3	Tobacco3482	CLS	Acc	92.43	61.14	<b>93.38</b>	<b>92.14</b>	91.62	37.90	<b>78.86</b>	<b>13.57</b>	<b>31.28</b>
Average CLS				88.63	64.16	87.45	85.46	83.47	48.78	71.89	16.75	24.47
Cascade R-CNN	DocLayNet-DLA	DLA	AP	49.74	10.39	<b>50.20</b>	36.96	36.16	13.76	<b>19.55</b>	30.19	39.35
Faster R-CNN	DocLayNet-DLA	DLA	AP	50.03	6.60	48.47	<b>37.33</b>	35.42	7.89	17.84	32.19	43.43
Cascade R-CNN	ICDAR2019	DLA	AP	87.69	64.06	<b>91.13</b>	84.08	<b>88.09</b>	67.48	<b>84.65</b>	3.05	23.64
Faster R-CNN	ICDAR2019	DLA	AP	85.52	62.10	88.56	82.64	85.04	71.37	83.26	2.26	23.42
Cascade R-CNN	PubLayNet	DLA	AP	<b>90.84</b>	62.25	90.97	<b>88.95</b>	87.92	<b>77.97</b>	78.06	12.78	28.59
Faster R-CNN	PubLayNet	DLA	AP	85.72	58.94	85.70	82.93	82.36	71.85	72.84	12.88	26.78
Average DLA				74.92	44.06	75.84	68.81	69.17	51.72	59.37	<b>15.56</b>	<b>30.87</b>
Average all				72.21	51.15	72.73	67.79	68.66	50.37	62.76	<b>9.45</b>	<b>21.06</b>

Table 3: Performance across datasets and tasks with three training settings: (1) Full: models trained on all real (R), all synthetic (S), or both (R+S); (2) Few<sub>A</sub>: 300–1000 real samples with/without synthetic augmentation; (3) Few<sub>B</sub>: 100 real samples with/without synthetic augmentation. Gap columns (Δ) report:  $R_{Full} - (R+S)_{Few_B}$  (how close 100 augmented samples approaches full training) and  $R_{Full} - S_{Full}$  (real vs synthetic quality). Bold indicates best per setting (std < 0.02). Synthetic augmentation achieves +12.38 average improvement in Few<sub>B</sub> scenarios.

Synthetic augmentation proves most valuable in data-scarce settings. In Setting Few<sub>B</sub> with only 100 real samples, adding synthetic data yields +12.38 average improvement, bringing performance within 9.45 points of full real-data training. This demonstrates substantial annotation cost reduction: augmenting minimal labeled data with synthetic samples achieves 87% of full-dataset performance.

#### 4.4 Visual Quality Comparison

Tab. 4 shows our framework achieves strong visual fidelity across diverse document types, with Layout-FID [21] scores below 10 for most datasets: WTQ (3.13), DocLayNet (6.35–6.45), DocVQA (6.96), and KLC (7.98). Performance on CORD is noticeably worse (36.46 Layout-FID, 139.52 FID). However, this is expected as CORD consists of camera-captured receipt images that contain real-world artifacts such as blur, lighting variation, and complex real-world backgrounds.

While direct comparison is challenging due to the different nature of setting across multiple document synthesis frameworks (as in Tab. 1), we also compare the FID scores achieved by our approach with multiple existing works [21,5,56,15]. Against DocGenie [21], which we extend, our approach achieves lower FID on CORD (139.52 vs. 155.34) and SROIE (63.50 vs. 109.31), though DocGenie reports superior Layout-FID on these datasets (31.30 vs. 36.46 on CORD; 3.52 vs. 17.18 on SROIE)<sup>5</sup>. Note that our CC sampling with  $\alpha = 1$  replicates DocGenie’s [21] seed-guided generation strategy; however, DocGenie uses 10 seeds, while we use 6 seeds for these datasets with prompting optimized for GT generation. Other methods [5,56,15] which are mostly diffusion-based achieve better FID scores on PubLayNet (33.75 at  $128 \times 128$ , 15.02 at  $256 \times 256$  vs. our 35.28 at full resolution) and DocLayNet-DLA (20.58 at  $256 \times 256$  vs. 37.80) but this is expected since all these approaches synthesize new documents by training on the training distribution of the same dataset. Furthermore, these approaches typically synthesize at lower resolutions ( $128 \times 128$  to  $256 \times 256$ ) and require ground truth layout annotations as input, fundamentally differing from our annotation-free approach. Our framework trades some visual fidelity for complete annotated dataset synthesis from unlabeled documents, enabling direct supervised learning across multiple tasks. For additional qualitative visual results of our framework, refer to Appendix I.

#### 4.5 Analysis of Failure-Cases

While synthetic data improves few-shot performance and maintains competitive full-shot results (Tab. 3), qualitative analysis reveals systematic failure modes. For KIE, despite reasonable spatial distributions (Appendix K.3), synth-only achieves 49–72 F1 vs. 88–95 real. Real samples are camera captures with scanning artifacts and distortions absent in pristine synthetic documents; CORD additionally applies artificial selective blur to non-KIE regions. Unlike DocGenie [21], which applies synthetic degradation post-generation, our focus on multi-task GT generation produces clean documents, creating a visual domain gap evidenced by LayoutLMv3 degrading on FUNSD (88.56→87.74 F1) while text-only models improve. For CLS, severe class imbalance (Fig. 24 in Appendix)

<sup>5</sup> DocGenie [21] is closed-source, preventing verification of their exact Layout-FID computation. FID-based metrics can be sensitive to sample size and implementation details. We compute Layout-FID using LayoutLMv3 CLS token embeddings, which may differ from DocGenie’s unspecified approach.

Dataset	Method	Task	FID (↓)	LayoutFID (↓)
DocVQA	Ours	VQA	41.36	6.96
WTQ	Ours	VQA	52.43	3.13
CORD	DocGenie [21]	KIE	155.34	31.30
	Ours	KIE	139.52	36.46
FUNSD	Ours	KIE	44.57	9.60
KLC	Ours	KIE	26.98	7.98
SROIE	DocGenie [21]	KIE	109.31	3.52
	Ours	KIE	63.50	17.18
RVL-CDIP	Ours	CLS	86.59	8.82
Tobacco3482	Ours	CLS	61.86	14.43
DocLayNet-CLS	Ours	CLS	36.62	6.45
PubLayNet	DocSynth [5]	DLA 33.75 @ 128 × 128	-	-
	Tanveeret al. [56]	DLA 15.02 @ 256 × 256	-	-
	Feniret al. [15]	DLA 248 @ 256 × 256	-	-
ICDAR2019	Ours	DLA	35.28	2.50
	Ours	DLA	43.52	7.19
DocLayNet-DLA	Tanveeret al. [56]	DLA 20.58 @ 256 × 256	-	-
	Ours	DLA	37.80	6.35

Table 4: FID [24] and Layout-FID [21] scores comparing our method to prior work. Lower scores indicate better distributional similarity to real documents. Resolution annotations indicate synthesis resolution before upscaling for evaluation.

yields synth-only accuracy of 44–61% vs. 76–92% real, with VLMs generating memos ( $\sim 45\%$ ) while neglecting specialized classes ( $< 2\%$ ). For DLA, synth-only achieves 6–10 AP vs. 49–50 real; however, qualitative analysis confirms reasonable predictions, indicating low scores stem from annotation inconsistencies rather than synthesis failure. Overall, GT analysis (Appendix K) validates high semantic and spatial annotation quality - question embeddings align closely between real and synthetic samples, and spatial entity distributions are well-preserved - though class imbalance remains a limitation for classification tasks. Manual inspection reveals  $\sim 3\%$  of documents across all tasks exhibit rendering failures or anomalous layouts.

#### 4.6 Discussion

Our experiments demonstrate that VLM-based synthesis generates high-quality document distributions suitable for model training. Synthetic-only training achieves 70.8% of real-data performance on average (51.15% vs. 72.21%), closely approximating real data on several datasets with gaps as small as 2.41 points (KLC [55]) and 5.05 points (DocVQA [38]). Combining real and synthetic data consistently improves results: +0.51 in full-shot and +0.83 in few-shot with 300 – 1000 samples. Most notably, augmenting only 100 real samples with synthetic data yields +12.38 improvement, achieving 87% of full real-data performance and demonstrating substantial annotation cost reduction. Seed selection analysis (Tab. 2) confirms that intra-cluster sampling with  $\alpha = 1$  (59.72% vs. 56.91%) preserves structural coherence more effectively than cross-cluster approaches.

To assess reproducibility with open-weight models, we additionally evaluate Gemma 3 27B (Appendix A). While it achieves comparable visual quality when successful (e.g., similar FID/Layout-FID), pipeline success rates are significantly lower — particularly for GT generation — reflecting instruction-following lim-

itations in current open-source VLMs rather than framework constraints. As open-weight VLMs continue to improve, we expect this gap to narrow, making our framework fully reproducible without proprietary models.

Though successful, challenges persist: pristine synthetic documents lack real-world degradations that vision encoders utilize, class imbalance emerges in classification tasks, and annotation taxonomy differences affect DLA scores despite qualitatively reasonable predictions. Integrating document degradation techniques (as in DocGenie [21]) with our GT generation framework could address visual domain gaps, while constrained sampling strategies could improve class balance. Overall, our framework offers a scalable, privacy-preserving approach that substantially reduces annotation costs while maintaining competitive performance across document understanding tasks.

## 5 Conclusion

We present a scalable framework for synthetic document generation that addresses labeled data scarcity in document understanding through VLM-based content generation, automatic ground truth annotation from unlabeled seed documents, and intelligent clustering-based seed selection. Our approach produces visually realistic documents with task-specific annotations across VQA, KIE, CLS, and DLA tasks. We release 140K+ synthetic samples across eleven datasets and DocVQA-HW to support other researchers.

Comprehensive evaluation demonstrates substantial annotation cost reduction: 100 real samples augmented with synthetic data achieves 87% of full real-data performance. Synthetic-only training reaches competitive performance compared to real data, while Layout-FID scores predominantly below 10 validate strong visual fidelity across diverse document types. Our clustering-based seed selection with intra-cluster sampling effectively preserves structural coherence and target distributions.

Future work should integrate existing degradation techniques (as in DocGenie [21]) with our multi-task GT generation framework to bridge the visual domain gap, implement constrained sampling strategies to address class imbalance, and explore content-aware generation for all visual element types. We are convinced that our framework helps accelerate data-efficient document understanding research and enables practitioners to train competitive models with minimal annotation costs.

**Acknowledgments.** This work was partially funded by the German Federal Ministry of Education and Research (BMBF).

**Disclosure of Interests.** The authors have no competing interests to declare that are relevant to the content of this article.

## References

1. Abarca, P.M., et al.: Synthetic document generation with full annotation: A framework utilizing open-weight large language models. In: Bagley, S.R., Simske, S.J.,

- Curtis, C., Mahlow, C. (eds.) Proc. ACM Symposium on Document Engineering. Nottingham, UK (Sep 2025), article no. 31
2. Askari, A., et al.: Expand, highlight, generate: RL-driven document generation for passage reranking. In: Bouamor, H., Pino, J., Bali, K. (eds.) EMNLP. pp. 10087–10099. Singapore (Dec 2023)
  3. Bauer, A., et al.: Comprehensive exploration of synthetic data generation: A survey. arXiv:2401.02524v2 [cs.LG] (Feb 2024)
  4. Belcák, P., et al.: Small language models are the future of agentic ai. ArXiv **abs/2506.02153** (2025), <https://api.semanticscholar.org/CorpusID:279119702>
  5. Biswas, S., et al.: DocSynth: A layout guided approach for controllable document image synthesis. In: Lladós, J., Lopresti, D., Uchida, S. (eds.) Document Analysis and Recognition - ICDAR 2021, LNCS, vol. 12823, pp. 555–568. Springer, Cham (2021)
  6. Biten, A.F., et al.: Scene text visual question answering. In: ICCV. pp. 4290–4300. Seoul, South Korea (Oct 2019)
  7. Brown, T.B., et al.: Large language models are few-shot learners. In: NIPSconf. NIPS, vol. 33, pp. 1877–1901. virtual (Dec 2020)
  8. Bui, Q.A., et al.: Automatic synthetic document image generation using generative adversarial networks: Application in mobile-captured document analysis. In: ICDAR. pp. 393–400. Sydney, Australia (Sep 2019)
  9. Cai, Z., et al.: Cascade R-CNN: High quality object detection and instance segmentation. PAMI **43**(5), 1483–1498 (May 2021)
  10. Campello, R.J.G.B., et al.: Density-based clustering based on hierarchical density estimates. In: Pei, J., Tseng, V.S., Cao, L., Motoda, H., Xu, G. (eds.) Advances in Knowledge Discovery and Data Mining, LNCS, vol. 7819, pp. 160–172. Springer, Berlin, Heidelberg (2013)
  11. Comanici, G., et al.: Gemini 2.5: Pushing the frontier with advanced reasoning, multimodality, long context, and next generation agentic capabilities. arXiv:2507.06261v5 [cs.CL] (Oct 2025)
  12. Dai, G., et al.: One-DM: One-shot diffusion mimicker for handwritten text generation. In: Leonardis, A., Ricci, E., Roth, S., Russakovsky, O., Sattler, T., Varol, G. (eds.) Computer Vision - ECCV 2024, LNCS, vol. 15116, pp. 410–427. Springer, Cham (2024)
  13. Devlin, J., et al.: BERT: Pre-training of deep bidirectional transformers for language understanding. In: Burstein, J., Christy, D., Thamar, S. (eds.) ACL. pp. 4171–4186. Minneapolis, MN (Jun 2019)
  14. Ding, C., et al.: SynthDoc: Bilingual documents synthesis for visual document understanding. In: Proc. 2nd Workshop on Large Generative Models Meet Multimodal Applications. pp. 16–25. Melbourne, Australia (Oct 2024)
  15. Fennir, T., et al.: Using GANs for domain adaptive high resolution synthetic document generation. In: Coustaty, M., Fornés, A. (eds.) Document Analysis and Recognition - ICDAR 2023 Workshops, LNCS, vol. 14193, pp. 49–61. Springer, Cham (2023)
  16. Fix, E., et al.: Discriminatory analysis: Nonparametric discrimination: Consistency properties. Tech. rep., USAF School of Aviation Medicine, Randolph Field, TX (1951)
  17. Futeral, M., et al.: mOSCAR: A large-scale multilingual and multimodal document-level corpus. arXiv:2406.08707v2 [cs.CL] (May 2025)
  18. Gao, L., et al.: ICDAR 2019 competition on table detection and recognition (cT-DaR). In: ICDAR. pp. 1510–1515. Sydney, Australia (Sep 2019)

19. Gupte, A., et al.: Lights, camera, action! A framework to improve NLP accuracy over OCR documents. arXiv:2108.02899v1 [cs.CL] (Aug 2021)
20. Hamdani, S.J.H., et al.: Latent diffusion for guided document table generation. In: Smith, E.H.B., Liwicki, M., Peng, L. (eds.) Document Analysis and Recognition - ICDAR 2024, LNCS, vol. 14808, pp. 368–383. Springer, Cham (2024)
21. Harikrishnan, P.M., et al.: DocGenie: A framework for high-fidelity synthetic document generation via seed-guided multimodal LLM and document-aware evaluation. In: CVPRW. Nashville, TN (Jun 2025)
22. Harley, A.W., et al.: Evaluation of deep convolutional nets for document image classification and retrieval. In: ICDAR. pp. 991–995. Nancy, France (Aug 2015)
23. He, L., et al.: Diffusion-based document layout generation. In: Fink, G.A., Jain, R., Kise, K., Zanibbi, R. (eds.) Document Analysis and Recognition - ICDAR 2023, LNCS, vol. 14187, pp. 361–378. Springer, Cham (2023)
24. Heusel, M., Ramsauer, H., Unterthiner, T., Nessler, B., Hochreiter, S.: Gans trained by a two time-scale update rule converge to a local nash equilibrium. In: NIPSconf. pp. 6626–6637 (2017)
25. Ho, J., et al.: Denoising diffusion probabilistic models. In: Larochelle, H., Ranzato, M., Hadsell, R., Balcan, M.F., Lin, H.T. (eds.) NIPSconf. NIPS, vol. 33, pp. 6840–6851. virtual (Dec 2020)
26. Hong, T., et al.: BROS: A pre-trained language model focusing on text and layout for better key information extraction from documents. In: AAAI. pp. 10767–10775. virtual (Feb 2022)
27. Hou, Q., et al.: Synthesizing realistic data for table recognition. In: Smith, E.H.B., Liwicki, M., Peng, L. (eds.) Document Analysis and Recognition - ICDAR 2024, LNCS, vol. 14804, pp. 367–388. Springer, Cham (2024)
28. Huang, Y., et al.: LayoutLMv3: Pre-training for document AI with unified text and image masking. In: Magalhães, J., Bimbo, A.D., Satoh, S., Sebe, N., Alameddini, X., Jin, Q., Oria, V., Toni, L. (eds.) Proc. 30th ACM International Conference on Multimedia. pp. 4083–4091. Lisboa, Portugal (Oct 2022)
29. Huang, Z., et al.: ICDAR2019 competition on scanned receipt OCR and information extraction. In: ICDAR. pp. 1516–1520. Sydney, Australia (Sep 2019)
30. Jaume, G., et al.: FUNSD: A dataset for form understanding in noisy scanned documents. In: 2nd International Workshop on Open Services and Tools for Document Analysis, OST@ICDAR 2019. pp. 1–6. Sydney, Australia (Sep 2019)
31. Journet, N., et al.: DocCreator: A new software for creating synthetic ground-truthed document images. *Ji* **3**(4) (Oct 2017), article no. 62
32. Karras, T., et al.: Analyzing and improving the image quality of StyleGAN. In: CVPR. pp. 8107–8116. virtual (Jun 2020)
33. Kim, G., et al.: OCR-free document understanding transformer. In: Avidan, S., Brostow, G., Cissé, M., Farinella, G.M., Hassner, T. (eds.) Computer Vision - ECCV 2022, LNCS, vol. 13688, pp. 498–517. Springer, Cham (2022)
34. Kumar, J., et al.: Structural similarity for document image classification and retrieval. *PRL* **43**, 119–126 (Jul 2014)
35. Li, J., et al.: LayoutGAN: Generating graphic layouts with wireframe discriminators. In: ICLR. New Orleans, LA (May 2019)
36. Lu, C., et al.: DPM-solver: A fast ODE solver for diffusion probabilistic model sampling in around 10 steps. In: Koyejo, S., Mohamed, S., Agarwal, A., Belgrave, D., Cho, K., Oh, A. (eds.) NIPSconf. NIPS, vol. 35, pp. 5775–5787. New Orleans, LA (Nov 2022)
37. Marti, U.V., et al.: The IAM-database: An english sentence database for offline handwriting recognition. *IJDAR* **5**(1), 39–46 (Nov 2002)

38. Mathew, M., et al.: Docvqa: A dataset for VQA on document images. In: WACV. Waikoloa, HI (Jan 2021)
39. McInnes, L., et al.: UMAP: uniform manifold approximation and projection. *J. Open Source Softw.* **3**(29) (2018), article no. 861
40. Nassar, A., et al.: TableFormer: Table structure understanding with transformers. In: CVPR. pp. 4614–4623. New Orleans, LA (Jun 2022)
41. Nikolaidou, K., et al.: Wordstylist: Styled verbatim handwritten text generation with latent diffusion models. In: Fink, G.A., Jain, R., Kise, K., Zanibbi, R. (eds.) *Document Analysis and Recognition - ICDAR 2023*, LNCS, vol. 14188, pp. 384–401. Springer, Cham (2023)
42. Park, S., et al.: CORD: A consolidated receipt dataset for post-OCR parsing. In: *Document Intelligence Workshop at NeurIPS*. Vancouver, Canada (Dec 2019)
43. Pasupat, P., et al.: Compositional semantic parsing on semi-structured tables. In: Zong, C., Strube, M. (eds.) *ACL*. pp. 1470–1480. Beijing, China (Jul 2015)
44. Pfizmann, B., et al.: DocLayNet: A large human-annotated dataset for document-layout segmentation. In: Zhang, A., Rangwala, H. (eds.) *Proc. 28th ACM SIGKDD Conference on Knowledge Discovery and Data Mining*. pp. 3743–3751. Washington, DC (Aug 2022)
45. Radford, A., et al.: Learning transferable visual models from natural language supervision. In: Meila, M., Zhang, T. (eds.) *ICML*. PMLR, vol. 139, pp. 8748–8763. virtual (Jul 2021)
46. Raffel, C., et al.: Exploring the limits of transfer learning with a unified text-to-text transformer. *JMLR* **21**(140), 1–67 (2020)
47. Raman, N., et al.: Synthetic document generator for annotation-free layout recognition. *PR* **128** (Mar 2022), article no. 108660
48. Reimers, N., et al.: Sentence-BERT: Sentence embeddings using siamese BERT-networks. In: Inui, K., Jiang, J., Ng, V., Wan, X. (eds.) *EMNLP*. pp. 3980–3990. Hong Kong, China (Nov 2019)
49. Ren, S., et al.: Faster R-CNN: towards real-time object detection with region proposal networks. *PAMI* **39**(6), 1137–1149 (Jun 2017)
50. Riaz, N., et al.: StylusAI: Stylistic adaptation for robust german handwritten text generation. In: Smith, E.H.B., Liwicki, M., Peng, L. (eds.) *Document Analysis and Recognition - ICDAR 2024*, LNCS, vol. 14805, pp. 429–444. Springer, Cham (2024)
51. Rombach, R., et al.: High-resolution image synthesis with latent diffusion models. In: CVPR. pp. 10684–10695. New Orleans, LA (Jun 2022)
52. Rousseeuw, P.J.: Silhouettes: A graphical aid to the interpretation and validation of cluster analysis. *Comp. & Appl. Math.* **20**(1), 53–65 (1987)
53. Sampaio, P.R., et al.: Unsupervised document and template clustering using multimodal embeddings. arXiv:2506.12116v2 [cs.CL] (Aug 2025)
54. Sohl-Dickstein, J., et al.: Deep unsupervised learning using nonequilibrium thermodynamics. In: Bach, F., Blei, D. (eds.) *ICML*. PMLR, vol. 70, pp. 2256–2265. Lille, France (Jul 2015)
55. Stanislawek, T., et al.: Kleister: Key information extraction datasets involving long documents with complex layouts. In: Lladós, J., Lopresti, D., Uchida, S. (eds.) *Document Analysis and Recognition - ICDAR 2021*, LNCS, vol. 12821, pp. 564–579. Springer, Cham (2021)
56. Tanveer, N., et al.: Diffusion models for document image generation. In: Fink, G.A., Jain, R., Kise, K., Zanibbi, R. (eds.) *Document Analysis and Recognition - ICDAR 2023*, LNCS, vol. 14189, pp. 438–453. Springer, Cham (2023)

57. Varab, D., et al.: SynthDoc: Bilingual documents synthesis for visual document understanding. In: Moens, M.F., Huang, X., Specia, L., Yih, S. (eds.) EMNLP. pp. 10150–10161. virtual (Nov 2021)
58. Wang, J., et al.: LiLT: A simple yet effective language-independent layout transformer for structured document understanding. In: Muresan, S., Nakov, P., Villavicencio, A. (eds.) ACL. pp. 7747–7757. Dublin, Ireland (May 2022)
59. Wang, P., et al.: Qwen2-VL: Enhancing vision-language model’s perception of the world at any resolution. arXiv:2409.12191v2 [cs.CV] (Oct 2024)
60. Zhong, X., et al.: PubLayNet: Largest dataset ever for document layout analysis. In: ICDAR. pp. 1015–1022. Sydney, Australia (Sep 2019)

## Supplementary Material

### A Claude vs. Gemma 3 27B Comparison

To improve reproducibility we’ve done formal evaluation with Gemma 3 27B (Tab. 5), which shows significantly lower pipeline success but comparable visual quality when successful—reflecting instruction-following limitations in current open-source VLMs, not framework constraints.

Dataset	Task	VLM	Pipeline Success (%)		Quality			
			GT	SP	Vis FID ↓	LFID ↓	N	
DocVQA	VQA	Claude	<b>92.6</b>	<b>92.2</b>	<b>95.9</b>	<b>45.9</b>	<b>7.0</b>	6864
		Gemma	69.48	0.2	73.47	73.9	9.4	6864
FUNSD	KIE	Claude	<b>95.5</b>	<b>95.5</b>	<b>93.5</b>	<b>51.2</b>	<b>9.6</b>	140
		Gemma	71.9	0.0	71.1	83.2	11.2	134
RVL-CDIP	CLS	Claude	<b>91.6</b>	<b>97.1</b>	<b>98.6</b>	93.5	<b>10.6</b>	850
		Gemma	8.5	0.7	94.6	<b>93.4</b>	14.3	850
PubLayNet	DLA	Claude	<b>89.0</b>	<b>91.2</b>	<b>97.8</b>	<b>37.5</b>	<b>3.0</b>	1235
		Gemma	12.2	0.3	94.2	81.2	9.8	1235

Table 5: Claude vs. Gemma 3 27B comparison. **Pipeline Success:** GT = valid annotations, SP = single-page renders, Vis = valid visual element and handwriting definitions (documents without handwriting/visual elements are counted as valid). **Quality:** FID/LFID (Layout-FID) computed on N samples (lower = better).

### B Dataset Splits

Details on our dataset splits are given in Tab. 6. As discussed in Sec. 4, we limit training sets to 4,000 samples (except DocVQA, where we use the full train set to assess large-scale augmentation) to manage costs while maintaining sufficient data volume. This constraint reflects realistic resource limitations common in real-world applications.

Dataset	Train	Validation	Test	Train (Synth)
DocVQA [38]	10194	1286	1287	8082
DocVQA-HW	N/A	N/A	103	N/A
WTQ [43]	1350	337	421	1479
SROIE [29]	626	N/A	347	1008
FUNSD [30]	149	N/A	50	259
CORD [42]	800	100	100	1182
KLC [55]	3641	953	1309	3441
Tobacco3482 [34]	2782	N/A	700	4092
RVL-CDIP [22]	4000*	4000	39998	3819
DocLayNet-CLS [44]	4000*	1000*	4999	3978
DocLayNet-DLA [44]	4000*	1000*	4999	3732
PubLayNet [60]	4000*	11245	11405	3835
ICDAR2019 [18]	600	N/A	240	1515

\* For these datasets, we use a subset of the original training splits.

Table 6: Train/validation/test splits and synthetic training sets for all datasets used in our experiments. For datasets with no validation set, we use 5% of the training set as the validation set.

## C Embeddings and Clustering

To create the embeddings, we use the following checkpoints: `microsoft/layout-lmv3-base` for `layout` and `pooled`, `openai/clip-vit-base-patch32` for `clip`, and `all-mpnet-base-v2` for `sentence`.

We select the optimal clustering  $(\mathcal{E}^*, \kappa^*)$  by maximizing a heuristic quality score:

$$(\mathcal{E}^*, \kappa^*) = \arg \max_{\mathcal{E}, \kappa} [S(C_{\mathcal{E}, \kappa}) + H(C_{\mathcal{E}, \kappa})] \quad (2)$$

where  $S(C)$  is the silhouette score [52] measuring cluster compactness and  $H(C) = -\sum_{c=1}^K p_c \log p_c$  is normalized entropy measuring cluster balance (where  $p_c$  denotes a cluster’s proportion of the samples). This heuristic prioritizes clusterings with both high internal coherence and balanced cluster sizes, which aligns with

Embedding	$\kappa$	Rank Score $\uparrow$
combined	10	74
combined	5	72
sentence	5	65
clip	5	56
clip	10	55
sentence	10	51
pooled	10	50
pooled	5	48
layout	10	35
layout	5	27

Table 7: Clustering configurations ranked using cumulative position scores over our base datasets.

Dataset	Embedding	$\kappa$	Num Clusters	Silhouette Score $\uparrow$	Norm. Entropy $\uparrow$	Final Score $\uparrow$
SROIE	combined	10	14	0.64	0.94	0.79
ICDAR2019	clip	5	9	0.64	0.82	0.73
WTQ	combined	5	50	0.41	0.95	0.68
CORD	combined	10	22	0.39	0.96	0.68
Tobacco3482	combined	10	31	0.42	0.93	0.67
DocLayNet	combined	10	48	0.51	0.82	0.66
RVL-CDIP	combined	10	49	0.38	0.92	0.65
FUNSD	combined	10	4	0.36	0.92	0.64
KLC	combined	10	41	0.35	0.86	0.61
PubLayNet	clip	5	106	0.30	0.89	0.60
DocVQA	sentence	5	408	0.41	0.96	0.69
DocVQA	combined	5	362	0.37	0.96	0.67
DocVQA	sentence	10	192	0.39	0.92	0.66
DocVQA	combined	10	187	0.37	0.94	0.65
DocVQA	pooled	5	370	0.35	0.95	0.65
DocVQA	pooled	10	181	0.35	0.94	0.65
DocVQA	clip	10	123	0.33	0.91	0.62
DocVQA	clip	5	259	0.29	0.91	0.60
DocVQA	layout	5	282	0.25	0.95	0.60
DocVQA	layout	10	128	0.23	0.93	0.58

Table 8: Metrics of the selected clusterings for all datasets (top) and listing of all clusterings for DocVQA (bottom), where we used `combined` embeddings and  $\kappa = 10$  for our experiments.

our manual inspection showing that such configurations produce semantically meaningful, interpretable document groupings suitable for seed selection.

Configurations  $(\mathcal{E}, \kappa)$  are ranked using cumulative position scores: on each dataset, the top  $N$  configurations receive points from  $N$  down to 1 based on their composite metric ranking. Final rankings aggregate these scores across all datasets as  $R(\mathcal{E}, \kappa) = \sum_d r_d(\mathcal{E}, \kappa)$  and are listed in Sec. C. Based on these rankings and manual inspection we select a clustering configuration  $(\mathcal{E}^*, \kappa^*)$  for each dataset. Metrics for the selected configurations and metrics for all configurations on DocVQA [38] are shown in Sec. C, with the corresponding clusters visualized in Figs. 4 and 5.

## D Implementation Details for Handwriting Synthesis

**Dataset Preparation.** All experiments were conducted using the IAM handwriting dataset. Each word image was center-padded to a fixed spatial size of  $128 \times 512$  pixels without resizing to ensure consistent scale across all samples. This dimension covers over 95% of IAM words and aligns with the  $8 \times$  spatial reduction of the VAE encoder, yielding latent tensors of size  $[4, 16, 64]$ . Each image was encoded to the latent space using the pretrained `stabilityai/sd-vae-ft-mse` autoencoder with a scaling factor of 0.18215. The LMDB dataset stored per-sample latent, grayscale image, writer ID, and text transcription.

**Model Architecture.** The baseline model is a conditional latent diffusion model trained on VAE-encoded handwriting latents. The denoising network is a conditional UNet with cross-attention layers and residual blocks, conditioned jointly on text and writer identity. The text conditioning network is a transformer encoder with hidden dimension  $d = 512$ ,  $L = 6$  layers,  $H = 8$  attention heads, feedforward width  $d_{ff} = 2048$ , and dropout rate 0.1. The UNet operates

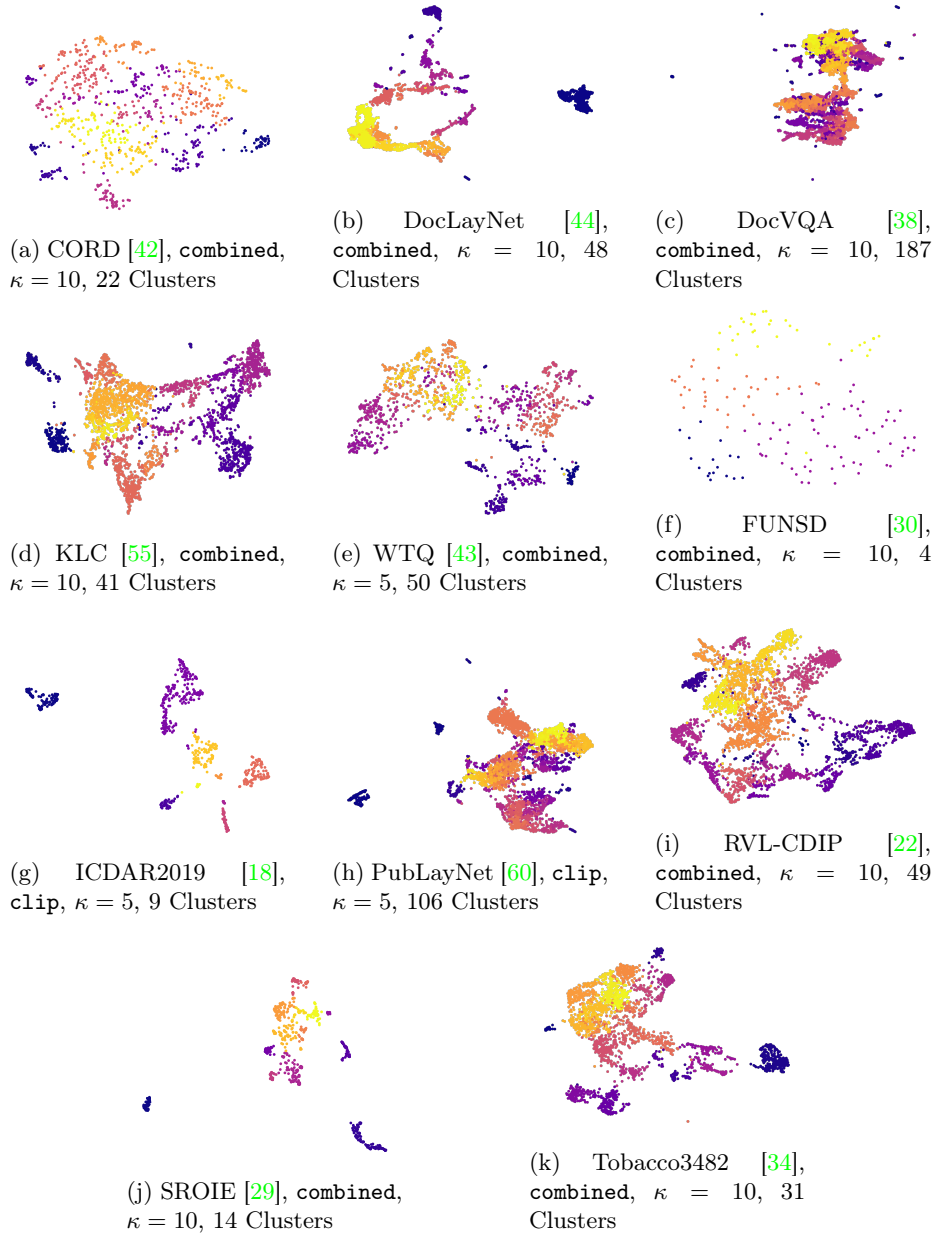


Fig. 4: Overview of our used clusters for all datasets. Each clustering lists embedding type, HDBSCAN [10] minimum cluster size  $\kappa$  and number of resulting clusters.

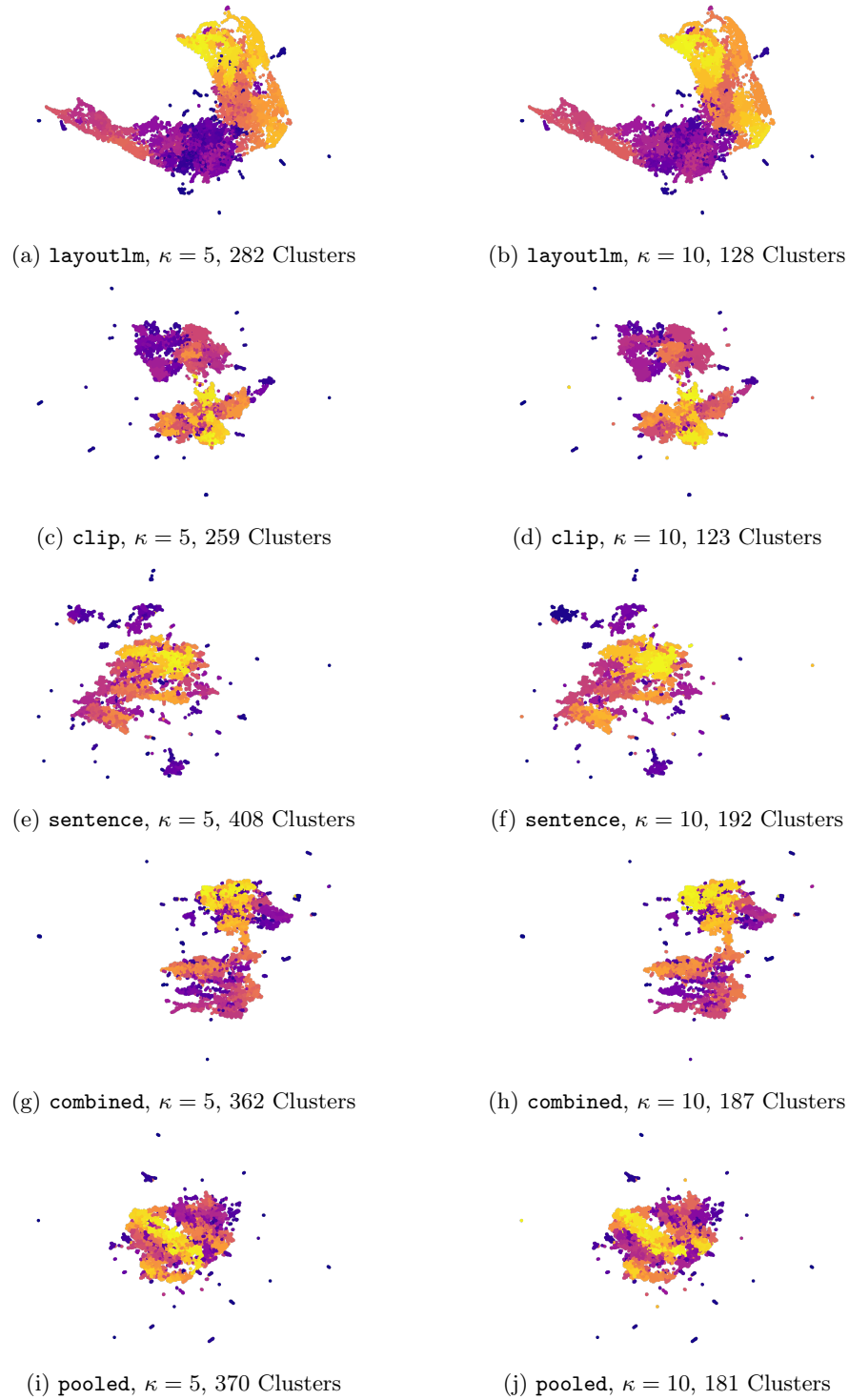


Fig. 5: Clustering results across different embeddings and HDBSCAN [10] minimum cluster sizes  $\kappa$  for DocVQA [38].

---

**Algorithm 1** Percentile Baseline Estimation

---

**Require:** RGBA segment image  $\tilde{I}$ ; opacity threshold  $\tau$ ; fixed percentile  $p = 50$ **Ensure:** Robust baseline  $b^*$ 

- 1: Extract alpha channel  $A$ ; let  $\mathcal{C}$  be columns with any pixel  $A > \tau$
  - 2: **for** each column  $j \in \mathcal{C}$  **do**
  - 3:      $b_j \leftarrow$  lowest row index with  $A(r, j) > \tau$
  - 4: **end for**
  - 5:  $b^* \leftarrow$  percentile ( $\{b_j\}_{j \in \mathcal{C}}, p$ )
  - 6: **return**  $b^*$
- 

on  $4 \times 16 \times 64$  latent inputs and includes class embeddings for writer conditioning. The diffusion scheduler follows the DDPM formulation with 1000 timesteps and a linear  $\beta$  schedule from  $\beta_{start} = 1 \times 10^{-4}$  to  $\beta_{end} = 0.02$ .

**Training Hyperparameters.** The model was trained using AdamW optimizer with learning rate  $1 \times 10^{-4}$ ,  $\beta_1 = 0.9$ ,  $\beta_2 = 0.999$ , and weight decay 0.01. Gradient clipping was set to 1.0. A cosine learning rate schedule was employed across 200 epochs. Mixed-precision training used **fp16** with automatic gradient scaling. EMA of model weights was applied with decay 0.9999 and power 1.0. The batch size per GPU was 16, with gradient accumulation for an effective batch size of 64. Random seed was fixed to 42. No image augmentations were applied to preserve text legibility.

**Inference and Generation.** At inference time, handwriting was generated from text tokens and corresponding writer embeddings. Generation used 30 diffusion steps with a DPMSolver++ multistep scheduler (order 3) and a temperature of 0.5. The VAE decoder scaled latents by  $1/0.18215$  before decoding to image space. To ensure consistent scale and aspect ratio, all generations were performed directly at the  $128 \times 512$  resolution without any resizing. For variable-length text, words longer than six characters were internally divided into balanced subsegments before generation, as the IAM corpus has an average word length of approximately six characters. Each subsegment was decoded separately and horizontally concatenated after generation.

**Scaling and Alignment.** Two issues were explicitly addressed. (1) *Scaling*: generation scale was fixed to the canonical  $128 \times 512$  resolution to prevent variation in stroke thickness and character proportion. (2) *Alignment*: baseline alignment was used for horizontal stitching. The baseline position of each segment was estimated from the bottom 50th percentile of the ink mask, and subsegments were vertically aligned by matching these baselines before compositing. Refer to algorithm 1 for baseline calculation.

**Post-Processing.** To remove discretization artifacts and simulate pen spread, a Gaussian blur was applied with radius  $r \sim \mathcal{U}(0.35, 0.85)$ . An anti-aliasing pass was optionally performed using a downscale-upscale factor of 0.75. Additional postprocessing parameters included contrast multiplier 1.02, ink gamma 0.98, additive Gaussian noise  $\sigma = 0.35$  (pixel intensity units), and unsharp mask

*Quick Brown Fox Jumps Over 342 Lazy Dogs*

(a) Sentence-level synthesis with a common baseline (red) produced by our diffusion model.

baseline=95.0
baseline=94.0
baseline=90.0
baseline=77.0  
*Quick Brown Fox Jumps*  
baseline=89.0
baseline=89.0
baseline=74.0
baseline=76.0  
*Over 342 Lazy Dogs*

(b) Word-level segments with estimated baselines (blue dashed lines) used to align the final sentence.

**Fig. 6: Diffusion-based handwriting generation and baseline alignment.** (a) The model synthesizes the full sentence “Quick Brown Fox Jumps Over 342 Lazy Dogs” with a coherent global baseline. (b) For each word segment, we estimate a robust baseline which is then used to compose the globally aligned line.

parameters  $(r, p, t) = (0.5, 30, 2)$ . The blurred outputs were composited with the alpha channel preserved to maintain soft ink boundaries.

**Summary.** The overall pipeline consists of: dataset padding and latent encoding → conditional diffusion training → text-conditioned inference with sub-word segmentation → baseline alignment → Gaussian and anti-aliasing refinement. This design ensures uniform spatial scale, stable conditioning, and visually realistic handwriting suitable for integration into synthetic printed documents.

## E Implementation Details for Visual Elements

*Visual Element Rendering.* Each visual element type requires specialized rendering: **stamp** elements use custom text-based generators; **barcode** elements encode numeric content (or random values if non-numeric) using the python-barcode library; **logo**, **figure**, and **photo** elements sample from image banks generated with Gemini 2.5 Flash [11], with **photo** additionally incorporating synthetic faces from StyleGAN2 [32] via ThisPersonDoesNotExist.com.

To generate the image banks, we prompt Gemini 2.5 Flash with the following instructions for each element type:

- **figure:** “Create an arbitrary scientific figure without any visible text and any additional requests.”
- **logo:** “Create an arbitrary, abstract logo without any visible text and any additional requests.”

- **photo**: “Create an arbitrary photo without any visible text and any additional requests.”

The resulting images for **figure**, **logo** and **photo** are shown in Figs. 8 to 10, respectively.

*Type Mapping.* As a post-processing step, we map certain VLM-predicted types to canonical categories: **chart**, **diagram**, **plot**, **graph**, **illustration**, and **infographic**  $\rightarrow$  **figure**; **image**  $\rightarrow$  **photo**; **seal**  $\rightarrow$  **stamp**. While such mislabelings are rare, this mapping helps retain more synthesized documents. For DLA, we augment ground truth annotations with *Figure/Picture* regions where needed, ensuring consistency between layout structure and annotations.

## F Environmental Impact and Energy Estimates

We provide conservative estimates of the energy consumption and carbon footprint of this work.

**Model Training:** Training the DocDjinn models consumed approximately 2,507 GPU hours, corresponding to  $\sim 752$  kWh of energy. Using a carbon intensity of 0.385 kg CO<sub>2</sub>/kWh (typical for European grids), this results in approximately 290 kg CO<sub>2</sub>.

**VLM Inference:** Direct measurements for Claude Sonnet 4.5 are not yet available. Based on benchmarking of similar frontier models<sup>1</sup>, we conservatively estimate that our 533M-token workload consumed  $\sim 113$  kWh. Using a carbon intensity of 0.287 kg CO<sub>2</sub>/kWh (reported for Claude infrastructure<sup>1</sup>), this corresponds to approximately 33 kg CO<sub>2</sub>.

**Total Estimated Footprint:** The combined estimated carbon footprint is  $\sim 323$  kg CO<sub>2</sub>. These estimates are conservative and intended as upper bounds. Carbon offsets have been purchased through Climeworks to compensate for these emissions.

## G Prompt Templates

We employ two prompt templates that differ in how the VLM generates ground truth (GT), corresponding to the annotation granularity required by each task family:

**(1) Macro Template (Document-Level GT):** This template instructs the VLM to generate document-level GT for tasks such as VQA and simple KIE. The GT is embedded as a JSON object within `<script></script>` tags in the HTML, separate for each synthetic document. For instance, VQA tasks generate JSON in the form: `{"Q1": "A1", "Q2": "A2", ...}`, where keys are question

<sup>1</sup> Nidhal Jegham, Marwan F. Abdelatti, Lassad Elmoubarki, Abdeltawab M. Hendawi, "How Hungry is AI? Benchmarking Energy, Water, and Carbon Footprint of LLM Inference," *CoRR*, vol. abs/2505.09598, 2025.

texts and values are corresponding answers. The macro prompt template is provided below:

### Macro: Document level JSON annotations

You are an AI creating authentic HTML representations of documents based on seed images. Analyze the seed images for structural and semantic content and generate authentic variations. The generated documents will be printed.

#### ## Requirements

1. **Authenticity**: Reflect stylistic elements from seed images without copying text/layouts verbatim
2. **Format**: Single-page documents with dimensions appropriate to the document type
3. **Language**: {language}
4. **Static Only**: No animations, transitions, or dynamic effects

#### ## Technical

- Wrap each document in '<HTML>...</HTML>' tags, numbered sequentially
- Static CSS only for single-page layout
- Generate only minified CSS, HTML, JS.

#### ## Content Guidelines

- DO**: Adapt cultural elements, vary layouts/colors/typography, use static styling
- DON'T**: Copy text/code blocks, reuse identical sections, include dynamic effects

#### ## Handwritten Fields (if document type requires)

- Mark with class 'handwritten' and use regular text
- Apply no special styles to 'handwritten', except generously increased size, in line with realistic handwriting
- Assign author ID via class ('author1', 'author2', etc.) to

```

distinguish different people
- If the handwriting represents a
signature mark it additionally with
class 'signature'

## Visual Placeholders (if document
type requires)
- Insert '<div data-placeholder="type"
style="...">' for non-text elements at
appropriate positions
- Valid types are: stamp, logo, figure,
barcode, photo
- Add data-content attribute with
actual content description
- For stamps, use 'position:absolute;
z-index:10;' and specify 'top'
and 'right'
- Always provide appropriate dimensions
- Example: '<div data-placeholder=
"stamp" data-content="APPROVED
2024-03-15"
style="position:absolute;top:50mm;
right:20mm;width:35mm;height:35mm;
z-index:10;"></div>'
- Example: '<div data-placeholder="logo"
data-content="ACME Corp Logo"
style="width:150mm;height:100mm;">
</div>'

## Output Format
Generate minified HTML like this:
'''
1. <HTML><!DOCTYPE html><html ...
document 1 ... </html></HTML>
2. <HTML><!DOCTYPE html><html ...
document 2 ... </html></HTML>
...
'''

## Ground Truth
Generate ground truth as JSON in
'<script type="application/json"
id="GT">...</script>' tag.
Ground truth specification: {gt_type}
Ground truth must follow the
format: {gt_format}

## Quality Checklist
- [ ] Authentic variations without

```

```

verbatim copying from seed images
- [ ] Static styling only
(no animations or dynamic effects)
- [ ] Single-page format with
minified HTML/CSS
- [ ] Content in {language}
- [ ] GT JSON present, correctly
formatted and semantically coherent
- [ ] Visual elements are semantically
coherent

Generate {num_solutions} distinct
{doc_type} documents based on
{num_seed_images} seed images.

```

**(2) Micro Template (Element-Level GT):** This template instructs the VLM to generate element-level GT for tasks requiring fine-grained spatial annotations, such as DLA and complex KIE. The VLM assigns each applicable HTML element a class label from a predefined set `{gt_type}` to uniquely identify its semantic role. For example, all elements containing figures, images, or visuals are assigned the class "LE-FIGURE". The micro prompt template is provided below:

#### Micro: Element level annotations

```

You are an AI creating authentic HTML
representations of documents based on
seed images. Analyze the seed images for
structural and semantic content and
generate authentic variations.
The generated documents will be printed.

```

#### ## Requirements

1. **Authenticity**: Reflect stylistic elements from seed images without copying text/layouts verbatim
2. **Format**: Single-page documents with dimensions appropriate to the document type
3. **Language**: {language}
4. **Static Only**: No animations, transitions, or dynamic effects

#### ## Technical

- Wrap each document in `<HTML>...</HTML>` tags, numbered sequentially
- Static CSS only for single-page layout

```

- Generate only minified CSS, HTML,
JS.

## Content Guidelines
**DO**: Adapt cultural elements, vary
layouts/colors/typography, use static
styling
**DON'T**: Copy text/code blocks, reuse
identical sections, include dynamic
effects

## Handwritten Fields (if document
type requires)
- Mark with class 'handwritten'
and use regular text
- Apply no special styles to
'handwritten', except generously
increased size, in line with realistic
handwriting
- Assign author ID via class
('author1', 'author2', etc.) to
distinguish different people
- If the handwriting represents a
signature mark it additionally with
class 'signature'

## Visual Placeholders (if document
type requires)
- Insert '<div data-placeholder="type"
style="...">' for non-text elements at
appropriate positions
- Valid types are: stamp, logo, figure,
barcode, photo
- Add data-content attribute with
actual content description
- For stamps, use 'position:absolute;
z-index:10;' and specify 'top'
and 'right'
- Always provide appropriate dimensions
- Example: '<div data-placeholder=
"stamp" data-content="APPROVED
2024-03-15"
style="position:absolute;top:50mm;
right:20mm;width:35mm;height:35mm;
z-index:10;"></div>'
- Example: '<div data-placeholder="logo"
data-content="ACME Corp Logo"
style="width:150mm;height:100mm;">

```

```

</div>‘

## Output Format
Generate minified HTML like this:
‘‘‘
1. <HTML><!DOCTYPE html><html ...
document 1 ... </html></HTML>
2. <HTML><!DOCTYPE html><html ...
document 2 ... </html></HTML>
...
‘‘‘

## Ground Truth
Generate ground truth by assigning each
applicable element in HTML a class from
the list below to uniquely identify
its label:
{gt_type}
{gt_format}

## Quality Checklist
- [ ] Authentic variations without
verbatim copying from seed images
- [ ] Static styling only
(no animations or dynamic effects)
- [ ] Single-page format with
minified HTML/CSS
- [ ] Content in {language}
- [ ] GT labels via class annotations
are present and assigned to
correct elements
- [ ] Visual elements are semantically
coherent

Generate {num_solutions} distinct
{doc_type} documents based on
{num_seed_images} seed images.

```

Both templates are instantiated with five parameters: language, document type (`{doc_type}`), GT type (`{gt_type}`), GT format (`{gt_format}`), and the number of documents to generate (`{num_solutions}`), as described in Section 3.2.

## H Synthetic Dataset Definitions

Below we list the configurations for all synthetic datasets generated in this work. Each definition instantiates the prompt templates from Section G, specifying the Task Type (VQA, DLA, KIE, CLS), Prompt Type (JSON or Annotation), and prompt parameters in YAML format.

**Dataset Definition I: DocVQA**

Task Type: VQA  
 Prompt Type: JSON

---

```

num_solutions: 3
doc_type: "business and administrative"

gt_type: "Multiple questions about each document, with
         their answers taken verbatim from the document."
gt_format: '{"<Text of question 1>": "<Answer to
         question 1>", "<Text of question 2>": "<Answer to
         question 2>", ...}'

```

**Dataset Definition II: WTQ**

Task Type: VQA  
 Prompt Type: JSON

---

```

num_solutions: 3
doc_type: "semi-structures table"

gt_type: |
  Multiple complex question-answer pairs in everyday
  language that can be answered from the
  associated table, with their answers taken 
  verbatim from the document.
  Common Question Types:
  * Lookup: Finding specific cell values ("What is the
  capital of France?")
  * Aggregation: Counting, summing, averaging ("How
  many players scored over 20 points?")
  * Comparison: Finding max/min ("Which country has
  the largest population?")
  * Reasoning: Requiring multiple steps ("What team
  did the highest scorer play for?")
gt_format: '{"<Text of question 1>": "<Answer to
         question 1>", "<Text of question 2>": "<Answer to
         question 2>", ...}'

```

**Dataset Definition III: CORD**

Task Type: KIE  
 Prompt Type: annotation

```

num_solutions: 3
doc_type: "receipt"

gt_type: |
  (if applicable, provide as plaintext values from the
  document)
  // Menu items (multiple menu items are allowed)
  * "MENU_NM": The menu item name.
  * "MENU_NUM": The menu item number or identifier.
  * "MENU_UNITPRICE": The price per unit of the menu
  item.
  * "MENU_CNT": The quantity or count of the menu
  item.
  * "MENU_DISCOUNTPRICE": The discount amount
  applied to the menu item.
  * "MENU_PRICE": The final price of the menu item.
  * "MENU_ITEMSUBTOTAL": The subtotal for this menu
  item line.
  * "MENU_VATYN": The VAT indicator (yes/no) for the
  menu item.
  * "MENU_ETC": Other miscellaneous menu item
  information.
  * "MENU_SUB_NM": The name of a sub-item or
  modifier.
  * "MENU_SUB_UNITPRICE": The price per unit of the
  sub-item.
  * "MENU_SUB_CNT": The quantity of the sub-item.
  * "MENU_SUB_PRICE": The price of the sub-item.
  * "MENU_SUB_ETC": Other sub-item information.
  // Menu items that were canceled
  * "VOID_MENU_NM": The name of a cancelled or
  voided item.
  * "VOID_MENU_PRICE": The price of the cancelled
  item.
  // Generic receipt data
  * "SUB_TOTAL_SUBTOTAL_PRICE": The subtotal before
  additional charges.
  * "SUB_TOTAL_DISCOUNT_PRICE": The total discount
  amount.
  * "SUB_TOTAL_SERVICE_PRICE": The service charge or
  fee.
  * "SUB_TOTAL_OTHERSVC_PRICE": Other service
  charges.
  * "SUB_TOTAL_TAX_PRICE": The tax amount.
  * "SUB_TOTAL_ETC": Other subtotal information.
  * "TOTAL_TOTAL_PRICE": The final total amount on
  the receipt.

```

```

* "TOTAL_TOTAL_ETC": Other total-related
  information.
* "TOTAL_CASHPRICE": The amount paid in cash.
* "TOTAL_CHANGEPRICE": The change given back to
  the customer.
* "TOTAL_CREDITCARDPRICE": The amount paid by
  credit card.
* "TOTAL_EMONEYPRICE": The amount paid by
  electronic money or digital payment.
* "TOTAL_MENUTYPE_CNT": The count of different
  menu item types.
* "TOTAL_MENUQTY_CNT": The total quantity of all
  items ordered.

```

```

gt_format: | Group individual menu items in groups using
  the menu item enumerator class MENU_<idx> and a sub-
  field class from the list above (e.g. "MENU_1
  MENU_NM", "MENU_1 MENU_CNT", "MENU_2 MENU_NM", ...).
  For void/canceled menu items use the class "
  VOID_MENU" instead of the enumeration. For generic
  receipt data use the class "GENERIC".

```

#### Dataset Definition IV: FUNSD

Task Type: KIE  
 Prompt Type: annotation

```

num_solutions: 3
doc_type: "form"

gt_type: |
  keys and their values structured as QA pairs
  * "HEADER": The header of the question answer pair
  .
  * "QUESTION": The question i.e. a key.
  * "ANSWER": The answer i.e a value.
gt_format: |
  Group individual annotations in groups using the
  enumerator class PAIR_<idx> and a annotation
  class from the list above (e.g. "PAIR_1 QUESTION
  ", "PAIR_1 ANSWER", "PAIR_2 HEADER", ...).
  Ensure to annotate exact using spans, i.e. "
  QUESTION" element should not contain "ANSWER".

```

**Dataset Definition V: Kleister Charity**

Task Type: KIE  
 Prompt Type: JSON

```
num_solutions: 3
doc_type: "UK charity annual financial report"

gt_type: |
  keys and their values (if applicable, provide as
  plaintext values from the document):
  * "address__post_town": Post town of the address
    of the charitable organization.
  * "address__postcode": Postcode of the address of
    the charitable organization.
  * "address__street_line": Street line of the
    address of the charitable organization.
  * "charity_name": The name of the charitable
    organization.
  * "charity_number": The registered number of the
    charitable organization.
  * "income_annually_in_british_
    pounds": The annual income in British Pounds of
    the charitable organization.
  * "report_date": The reporting date of the annual
    document of the charitable organization.
  * "spending_annually_in_british_
    pounds": The annual spending in British Pounds of
    the charitable organization.
gt_format: '{"address__post_town": "<value>", "
  spending_annually_in_british_pounds": "<value>",
  ...}'
```

**Dataset Definition VI: SROIE**

Task Type: KIE  
 Prompt Type: JSON

```
num_solutions: 3
doc_type: "receipt"

gt_type: |
  keys and their values
  * "COMPANY": The company name.
  * "DATE": The date on the receipt.
  * "ADDRESS": The address of the company.
```

```

    * "TOTAL": The total amount.
gt_format: '{"COMPANY": "<value>", "DATE": "<value>", "
    ADDRESS": "<value>", "TOTAL": "<value>"}'

```

### Dataset Definition VII: DocLayNet (CLS)

Task Type: Classification  
 Prompt Type: JSON

```

num_solutions: 3
doc_type: "single A4 pages out of diverse business and
    technical"

gt_type: |
    document class label
    * financial_reports
    * scientific_articles
    * laws_and_regulations
    * government_tenders
    * manuals
    * patents
gt_format: 'JSON object {"label": "<class label>"}'

```

### Dataset Definition VIII: RVL-CDIP

Task Type: CLS  
 Prompt Type: JSON

```

num_solutions: 3
doc_type: "business correspondence and corporate"

gt_type: |
    document class label
    * letter
    * form
    * email
    * handwritten
    * advertisement
    * scientific report
    * scientific publication
    * specification
    * file folder
    * news article
    * budget
    * invoice

```

```

* presentation
* questionnaire
* resume
* memo
gt_format: 'JSON object {"label": "<class label>"}'

```

### Dataset Definition IX: Tobacco3482

Task Type: CLS  
 Prompt Type: JSON

```

num_solutions: 3
doc_type: "legal and corporate"

gt_type: |
  document class labels:
  * ADVERTISEMENT: Advertisement
  * EMAIL: Email
  * FORM: Form
  * LETTER: Letter
  * MEMO: Memo
  * NEWS_ARTICLE: News article
  * NOTE: Note/handwritten note
  * REPORT: Report
  * RESUME: Resume/CV
  * SCIENTIFIC: Scientific publication
gt_format: 'JSON object {"label": "<class label>"}'

```

### Dataset Definition X: Doclaynet (DLA)

Task Type: DLA  
 Prompt Type: annotation

```

num_solutions: 2
doc_type: "single A4 pages out of diverse business and
          technical"

gt_type: |
  * "LE-CAPTION": Text that accompanies and explains
                  figures, tables, or other visual elements,
                  typically appearing above or below the
                  referenced element.
  * "LE-FOOTNOTE": Supplementary notes or citations
                  placed at the bottom of a page, providing

```

```

        additional context or references to the main
        text, distinct from footers.
    * "LE-FORMULA": Mathematical equations, chemical
      formulas, or symbolic expressions, whether
      displayed inline or as standalone elements.
    * "LE-LIST-ITEM": Individual items within
      enumerated, bulleted, or definition lists,
      with each list item annotated separately
      rather than as a unified list structure.
    * "LE-PAGE-FOOTER": Recurring content at the
      bottom of pages such as page numbers,
      copyright notices, document identifiers, or
      footer text.
    * "LE-PAGE-HEADER": Recurring content at the top
      of pages including running headers, document
      titles, chapter names.
    * "LE-PICTURE": Photographs, diagrams, charts,
      graphs, illustrations, and other visual
      content excluding tables.
    * "LE-SECTION-HEADER": Section and subsection
      headings.
    * "LE-TABLE": Complete table structure including
      grid content, inline captions, and column/row
      headers as a unified element.
    * "LE-TEXT": Contains regular body text including
      paragraphs, abstracts, definitions,
      descriptions, and other primary textual
      content.
    * "LE-TITLE": The main document title appearing
      prominently at the beginning of the document,
      distinct from section headers.
gt_format:

```

#### Dataset Definition XI: ICDAR2019 cTDaR

```

Task Type: DLA
Prompt Type: annotation

```

```

num_solutions: 2
doc_type: "single A4 pages out of diverse modern digital
          -born and historical archival scanned"

gt_type: |
    * "LE-TABLE": Any tabular structure containing data
      organized in rows and columns. Include the
      complete table region from border to border.

```

```
gt_format:
```

### Dataset Definition XII: Publaynet

```
Task Type: DLA
Prompt Type: annotation
```

```
num_solutions: 2
doc_type: "single A4 pages out of one and two column
scientific article"

gt_type: |
  * "LE-TEXT": Contains regular body text including
    paragraphs, abstracts, authors, affiliations,
    keywords, footnotes, footer, references, and
    captions for figures and tables.
  * "LE-TITLE": Comprises all document titles and
    headings, article titles as well as standalone
    section or subsection headings that appear on
    their own line rather than inline with text.
  * "LE-TABLE": Denotes the main body content of
    tables, excluding captions and labels.
  * "LE-FIGURE": Indicates the main visual content of
    figures and illustrations, with multi-panel
    figures annotated as complete units rather than
    individual sub-figures.
  * "LE-LIST": Represents enumerated or bulleted list
    structures, with nested lists annotated as
    single unified objects.

gt_format:
```

## I Synthetic Dataset Samples

This section provides visual examples from all synthetic datasets specified in Section H. For each dataset, we display representative synthetic documents generated by the VLM-based synthesis pipeline in Figs. 11 to 22. The examples demonstrate the variety in layout, typography, and content while maintaining task-specific authenticity.

## J Synthetic Dataset Details

Tables 9 and 10 report generation statistics for all synthetic datasets, including sample counts, token usage, estimated API costs, and content composition

Task	Dataset Name	Embedding Type	Min. Cluster Size	Total Samples	Total Valid Samples	Input Tokens (M)	Output Tokens (M)	Cost (USD)	Avg. Words	Avg. HW Elems	Avg. Visual Elems
CLASSIFICATION	DocLayNet-CLS [44]	comb	10	4494	3978	4.08	7.48	124	407	0.052	0.334
	RVL-CDIP [22]	comb	10	4441	3823	5.16	5.34	96	206	1.466	0.371
	Tobacco3482 [34]	comb	10	5292	4092	6.24	6.49	116	251	2.042	0.435
DLA	DocLayNet-DLA [44]	comb	10	4502	3732	2.95	7.28	114	372	0.061	0.301
	ICDAR2019 [18]	img	5	1594	1515	2.01	2.89	49	297	0.004	0.048
	PubLayNet [60]	img	5	4476	3835	5.9	12.14	200	874	0	0.542
KIE	CORD [42]	comb	10	1200	1182	1.19	1.66	29	67	0.007	0.158
	KLC [55]	comb	10	4005	3441	4.92	4.91	88	146	0.194	0.282
	FUNSD [30]	comb	10	291	259	0.34	0.5	9	128	3.629	0.205
QA	SROIE [29]	comb	10	1050	1008	1.46	1.62	29	113	0.089	0.124
	DocVQA [38]	comb	10	9990	8082	10.66	14.3	246	173	2.37	0.31
	WTQ [43]	comb	5	1604	1479	1.13	3.13	50	204	0.059	0.381

Table 9: Overview of the final synthesized datasets using sampling strategy (v2) and sampling strength ( $\alpha = 1$ ) in our experiments. For each dataset, we report the embedding type (image-only or image+text), clustering and sampling parameters, total and valid sample counts, token usage, estimated generation cost, and average text/visual content statistics.

metrics. The first table shows our final configurations, while the second presents ablation variants across different sampling strategies and strengths.

## K Synthetic Ground Truth

We provide qualitative analysis of the ground truth generated by our VLM-based synthesis pipeline across all tasks. The visualizations validate semantic consistency, spatial coherence, and annotation quality of synthetic data compared to real datasets, while also revealing systematic limitations such as class imbalance in classification tasks.

### K.1 QA

Fig. 23 shows embeddings of question text and distributions of question types for DocVQA [38] and WTQ [43]. Question embeddings are retrieved with Sentence Transformers [48] and projected to two dimensions with UMAP [39]. Notably, the close alignment between real and synthetic question embeddings demonstrates that our VLM generates semantically similar questions *without ever observing real ground truth annotations*—the synthesis is guided only by seed document images and task-level prompt parameters describing the desired GT structure.

Task	Dataset Name	Embedding Type	Min. Cluster Size	Sample Strategy	Sample Alpha	Total Samples	Total Valid Samples	Input Tokens (M)	Output Tokens (M)	Cost (USD)	Avg. Words	Avg. HW Elems	Avg. Visual Elems
CLASSIFICATION	RVL-CDIP [22]	comb	10	v1	1	4500	3853	5.04	5.28	95	211	1.305	0.397
	RVL-CDIP [22]	comb	10	v1	0.75	4306	3860	4.82	5.08	91	212	1.257	0.415
	RVL-CDIP [22]	comb	10	v1	0.5	4491	3997	5.03	5.32	96	209	1.24	0.414
	RVL-CDIP [22]	comb	10	v2	1	4441	3823	5.16	5.34	96	206	1.466	0.371
	RVL-CDIP [22]	comb	10	v2	0.75	4329	3891	5.04	5.25	94	210	1.446	0.411
	RVL-CDIP [22]	comb	10	v2	0.5	4407	3860	5.16	5.33	95	206	1.31	0.411
DLA	PubLayNet [60]	img	5	v1	1	4469	3937	5.9	12.97	212	939	0	0.536
	PubLayNet [60]	img	5	v1	0.75	4476	3929	5.9	12.99	213	937	0	0.551
	PubLayNet [60]	img	5	v1	0.5	4481	3988	5.9	13.05	213	943	0	0.568
	PubLayNet [60]	img	5	v2	1	4476	3835	5.9	12.14	200	874	0	0.542
	PubLayNet [60]	img	5	v2	0.75	4505	3949	5.91	12.25	201	882	0	0.535
	PubLayNet [60]	img	5	v2	0.5	4497	3930	5.9	12.41	204	891	0	0.55
KIE	CORD [42]	comb	10	v1	1	1200	1187	1.18	1.67	27	68	0.008	0.133
	CORD [42]	comb	10	v1	0.75	1200	1193	1.18	1.68	29	70	0.008	0.14
	CORD [42]	comb	10	v1	0.5	1200	1191	1.17	1.66	29	68	0.01	0.145
	CORD [42]	comb	10	v2	1	1200	1182	1.19	1.66	29	67	0.007	0.158
	CORD [42]	comb	10	v2	0.75	1200	1174	1.19	1.66	29	67	0.009	0.15
	CORD [42]	comb	10	v2	0.5	1200	1185	1.18	1.67	27	68	0.007	0.163
QA	DocVQA [38]	comb	10	v1	1	10002	8463	10.6	14.63	251	167	2.659	0.318
	DocVQA [38]	comb	10	v1	0.75	10014	8463	10.55	14.71	252	164	2.752	0.315
	DocVQA [38]	comb	10	v1	0.5	10013	8501	10.52	14.77	253	162	2.847	0.307
	DocVQA [38]	comb	10	v2	1	9990	8082	10.66	14.3	246	173	2.37	0.31
	DocVQA [38]	comb	10	v2	0.75	10010	8345	10.59	14.53	250	168	2.364	0.328
	DocVQA [38]	comb	10	v2	0.5	9990	8088	10.55	14.6	251	167	2.666	0.315

Table 10: Ablation variants generated by varying the sampling strategy (v1/v2) and sampling strength ( $\alpha$ ). The table reports the same statistics as Table 9, enabling comparison of how sampling choices impact dataset size, token usage, and content composition.

Question type distributions are also well-preserved, indicating appropriate task coverage.

## K.2 CLS

Fig. 24 presents class distributions for RVL-CDIP [22], Tobacco3482 [34], and DocLayNet-CLS [44] classification datasets. The severe class imbalance in synthetic data is evident, with certain classes (e.g., memo) heavily overrepresented while specialized classes remain undersampled. This imbalance reflects both our intra-cluster sampling strategy with  $\alpha = 1$  that biases generation toward dominant document patterns, and the VLM’s tendency to more readily generate certain document types over others. This imbalance contributes to the performance gap observed in Section 4.5.

### K.3 KIE

Figs. 25 and 26 show spatial heatmaps comparing entity placement by type between real and synthetic data for CORD [42], FUNSD [30] and SROIE [29]. The heatmaps demonstrate that spatial distributions of key-value entities are well-preserved, validating the quality of element-level annotations generated by our micro template without access to real annotations.

### K.4 DLA

Figs. 32 and 33 present spatial heatmaps and region count distributions for IC-DAR2019 [18], PubLayNet [60] and DocLayNet-DLA [44]. While overall spatial layout patterns appear reasonable with region counts and positioning comparable to real data, detailed analysis of DocLayNet-DLA [44] predictions reveals both annotation taxonomy differences and synthesis limitations that explain the low quantitative scores: definitional mismatches in list-item classification (distance-based vs. semantic, see Fig. 28), insufficient variety in visual elements to capture complex images with embedded text (Fig. 29), limited table diversity in size and structure (Fig. 30), systematic labeling differences (e.g., chemistry formulas as "Formula" in synthetic data vs. "Picture" in real data) (Fig. 31), positional biases (top-left elements consistently labeled "Title" in synthetic data, while in real data they are often labeled as "Page Header" or "Section Header"), and near-complete failure on the "Caption" class. These findings indicate that performance gaps stem from both annotation inconsistencies and limitations in synthetic document diversity.

## L Evaluation Setup

Tab. 11 summarizes the default training configurations for all models and tasks used in our experiments. For each task (CLS, KIE, VQA, DLA) and model combination, we report learning rate, batch size, number of epochs, optimizer settings, regularization parameters, and other training details. These hyperparameters were selected based on preliminary experiments and follow common practices for document understanding tasks.

For training experiments in tasks CLS, KIE, and VQA, we fine-tune the BERT [13], LiLT [58], and LayoutLMv3 [28] models using their pretrained checkpoints: `bert-base-uncased`, `SCUT-DLVCLab/lilt-roberta-en-base`, and `microsoft/layoutlmv3-base`<sup>1</sup>, respectively. For the DLA task, we use the MMDetection<sup>2</sup> library to fine-tune the models using their available pretrained checkpoints.

<sup>1</sup> We use the pretrained checkpoints available at <https://huggingface.co/> for these models.

<sup>2</sup> <https://mmdetection.readthedocs.io/>

Task Model	Modality	Learning Rate	Batch Size	Epochs	Optimizer	Weight Decay	Momentum	Warmup Ratio	Dropout	Segment-Level Layout	Early Stopping	Mixed Precision	Image Size	
CLS	BERT [13]	T	1.00E-05	32	50	Adam	0.01	N/A	0.1	0.1	✗	✓	✗	N/A
	LiLT [58]	T+L	1.00E-05	32	50	Adam	0.01	N/A	0.1	0.1	✗	✓	✗	N/A
	LayoutLMv3 [28]	T+L+I	1.00E-05	32	50	Adam	0.01	N/A	0.1	0.1	✓	✓	✗	224×224
KIE	BERT [13]	T	2.00E-05	16	100	AdamW	0.01	N/A	0.1	0.1	✗	✗	✗	N/A
	LiLT [58]	T+L	2.00E-05	16	100	AdamW	0.01	N/A	0.1	0.1	✗	✗	✗	N/A
	LayoutLMv3 [28]	T+L+I	2.00E-05	16	100	AdamW	0.01	N/A	0.1	0.1	✓	✗	✗	224×224
VQA	BERT [13]	T	5.00E-05	32	50	Adam	0.01	N/A	0.02	0.1	✗	✓	✗	N/A
	LiLT [58]	T+L	5.00E-05	32	50	Adam	0.01	N/A	0.02	0.1	✗	✓	✗	N/A
	LayoutLMv3 [28]	T+L+I	5.00E-05	16	50	Adam	0.01	N/A	0.02	0.1	✓	✓	✗	224×224
DLA	Faster R-CNN [49]	I	2.00E-02	16	40	SGD	0.0001	0.9	0.05	0.1	✗	✓	✓	480–800×1333
	Cascade R-CNN [9]	I	2.00E-02	16	40	SGD	0.0001	0.9	0.05	0.1	✗	✓	✓	480–800×1333

Table 11: Default training hyperparameters for all models and tasks in our experiments. For each task (CLS, KIE, VQA, DLA) and model combination, we report learning rate, batch size, number of epochs, optimizer settings, and other training parameters. These settings were chosen based on preliminary experiments and common practices for document understanding tasks.

To reduce training time and computational overhead, we adopt early stopping<sup>3</sup> with a patience of 10 wherever specified. Specifically, we evaluate the model on the validation set after every training epoch, and if the target metric does not exceed its best value for 10 consecutive epochs, we terminate training early. However, for training configurations Few<sub>A</sub> (R) and Few<sub>B</sub> (R), since the dataset sizes are extremely small (100, 300, or 1000 samples), we disable early stopping and train for the full number of epochs for a fair comparison. Across all experiments, we use the validation set to select the best checkpoint and report test performance using the checkpoint that achieves the highest validation score.

## M Data & Code Availability

Complete source code is provided in this supplementary material, including the VLM-based synthesis pipeline, clustering and sampling procedures, model training scripts, and evaluation tools. Due to size constraints, we include representative samples of the synthetic datasets and the complete DocVQA-HW subset in the supplementary material. The full synthetic datasets (140K+ samples across eleven benchmarks) will be released upon publication. All real-world benchmark datasets are publicly available from their original sources as cited in the paper.

<sup>3</sup> Mahsereci, Maren, et al. "Early stopping without a validation set." arXiv preprint arXiv:1703.09580 (2017).

The figure displays several lines of handwritten text, each with small blue boxes above the words indicating segmentation. The text is as follows:

Ms. Patricia Caldwell  
Director of Operations  
Westfield Industries Ltd.  
450 Commerce Drive  
Portland OR 97204

Dear Ms. Caldwell

I am writing to express my appreciation for the  
opportunity to collaborate with your organization over  
the past eighteen months. The partnership has proven  
mutually beneficial and has exceeded initial projections.

Fig. 7: **Baseline-aligned handwriting synthesis.** The figure shows multiple handwriting segments generated by our latent diffusion model. Individually synthesized words, each with an automatically estimated baseline and composition of these word segments into globally baseline-aligned sentences, demonstrating consistent geometric structure across words and lines.

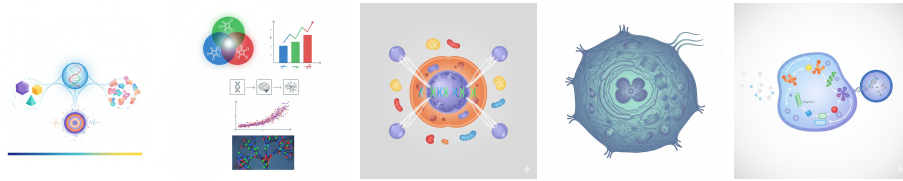


Fig. 8: Image bank for visual elements of type **figure**, generated with Gemini 2.5 Flash [11].



Fig. 9: Image bank for visual elements of type **logo**, generated with Gemini 2.5 Flash [11].



Fig. 10: Image bank for visual elements of type **photo**, generated with Gemini 2.5 Flash [11] (top). Synthetic faces (bottom) generated with StyleGAN2 [32] via ThisPersonDoesNotExist.com.

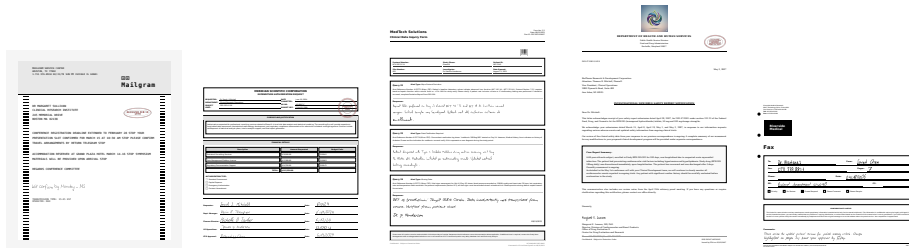


Fig. 11: DocVQA [38] synthetic dataset samples for VQA task.



Fig. 12: WTQ [43] synthetic dataset samples for VQA task.

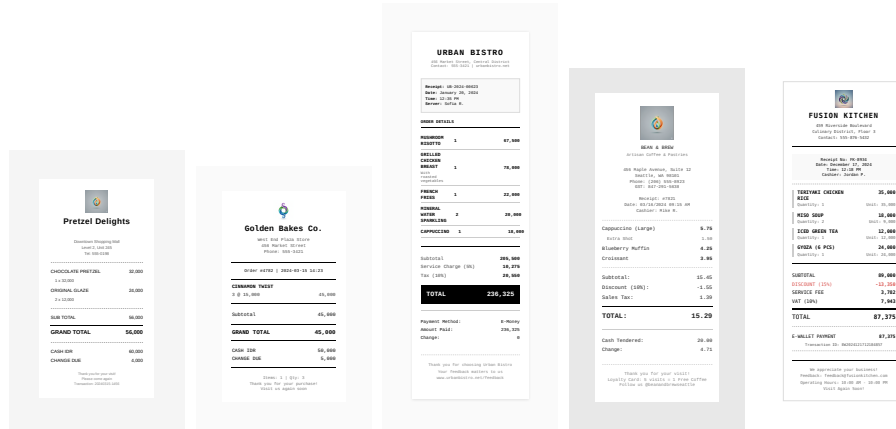


Fig. 13: CORD [42] synthetic dataset samples for KIE task.



Fig. 14: FUNSD [30] synthetic dataset samples for KIE task.



Fig. 15: KLC [55] synthetic dataset samples for VQA task.



Fig. 16: SROIE [29] synthetic dataset samples for KIE task.

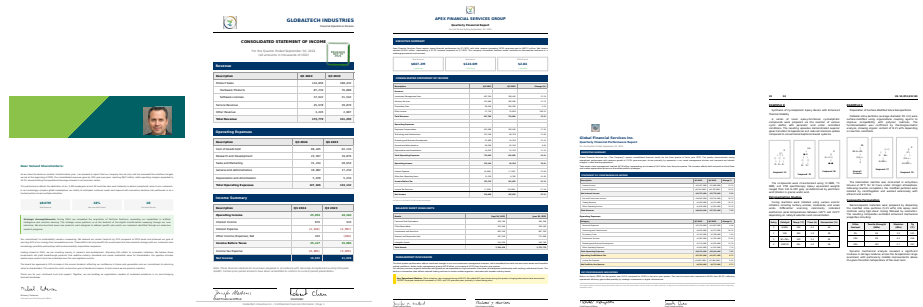


Fig. 17: DocLayNet-CLS [44] synthetic dataset samples for CLS task.

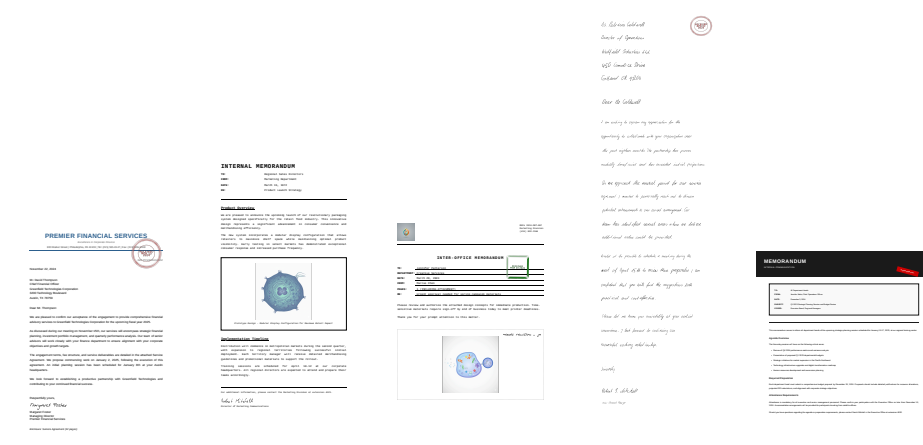


Fig. 18: RVL-CDIP [22] synthetic dataset samples for CLS task.

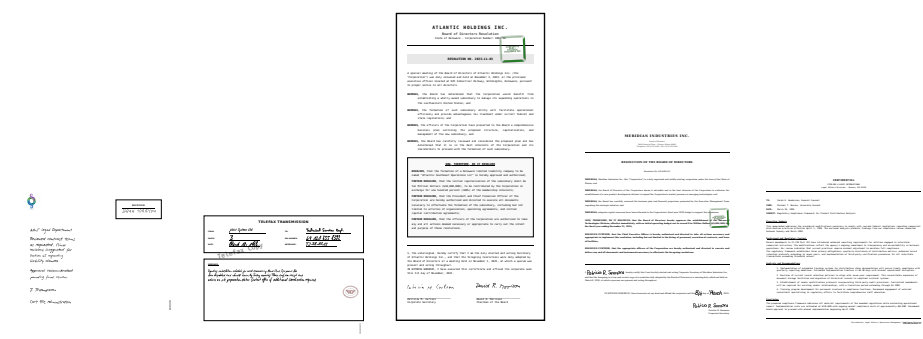


Fig. 19: Tobacco3482 [34] synthetic dataset samples for CLS task.



Fig. 20: DocLayNet-DLA [44] synthetic dataset samples for DLA task.

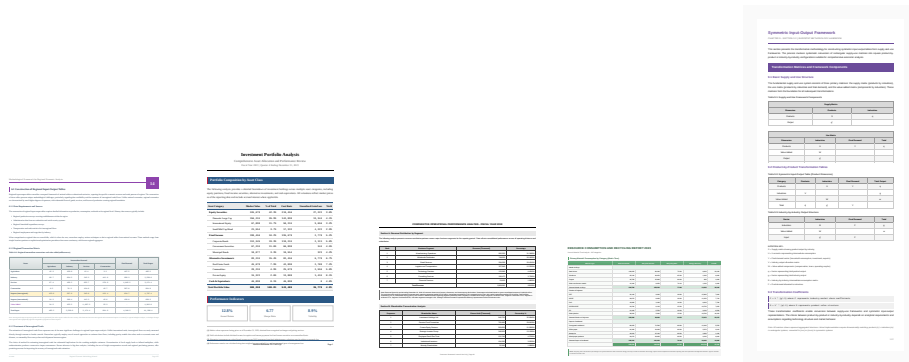


Fig. 21: ICDAR2019 [18] synthetic dataset samples for DLA task.

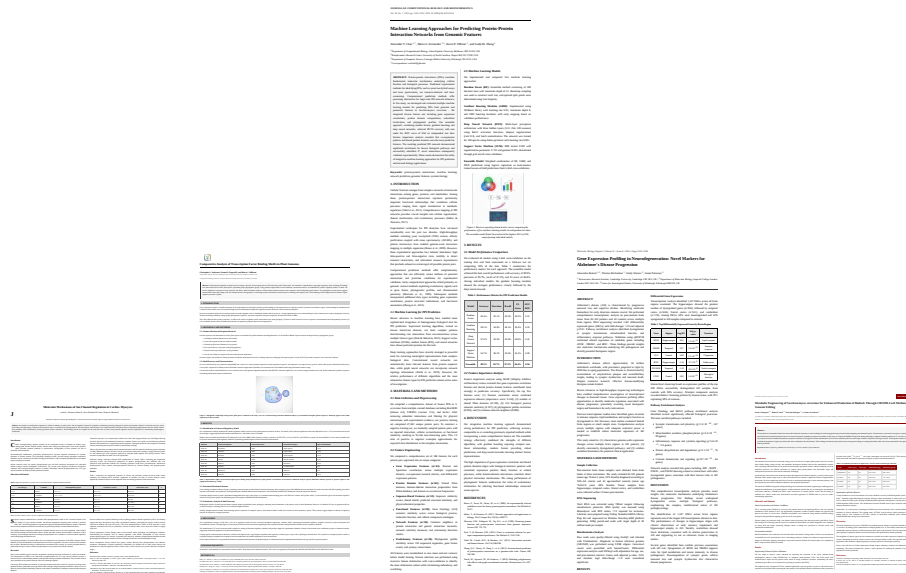


Fig. 22: PubLayNet [60] synthetic dataset samples for DLA task.

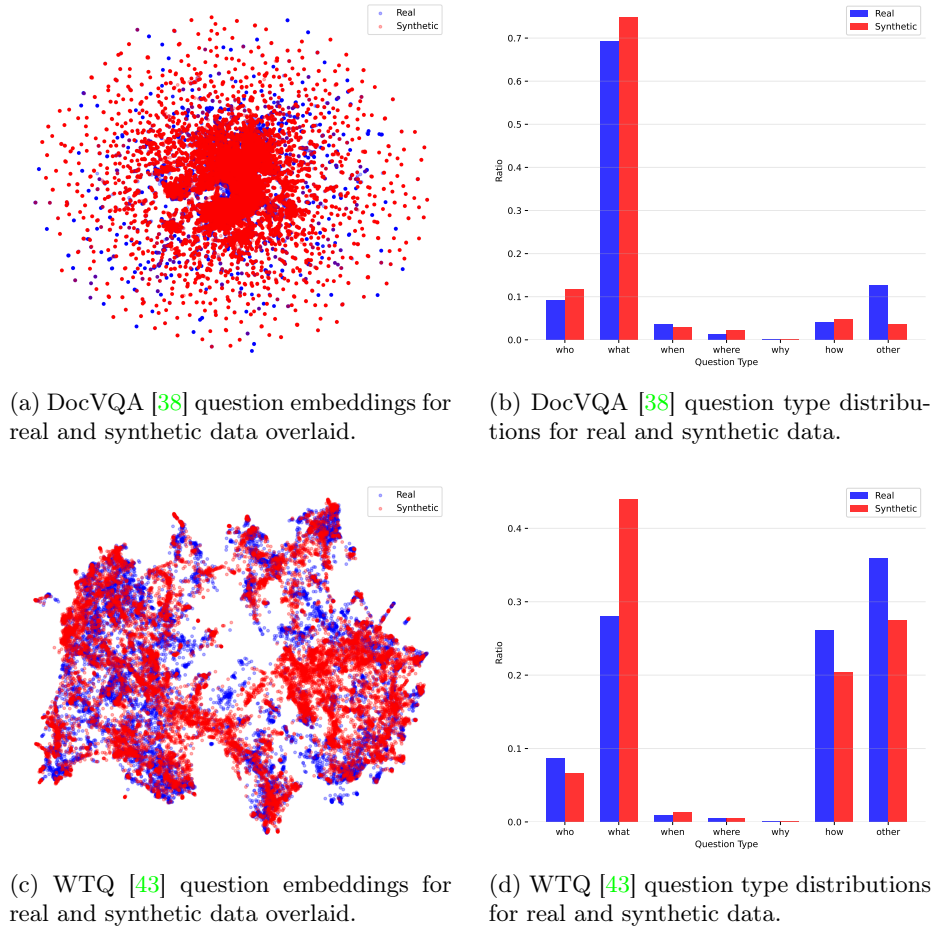
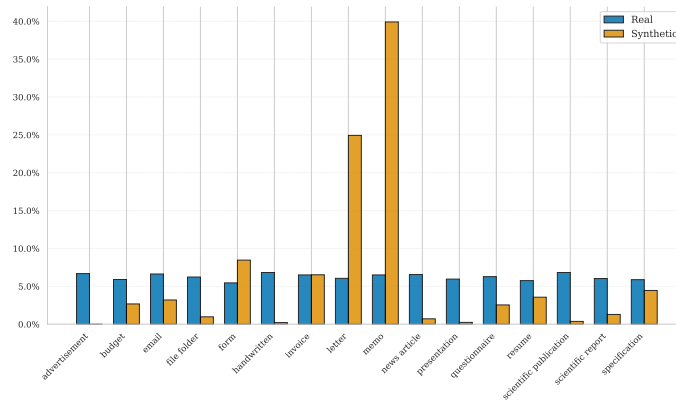
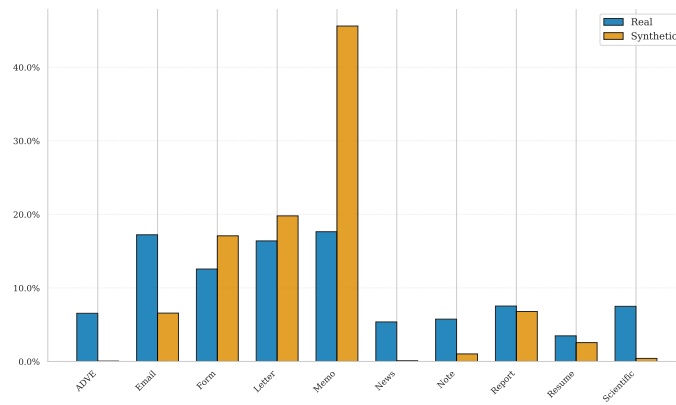


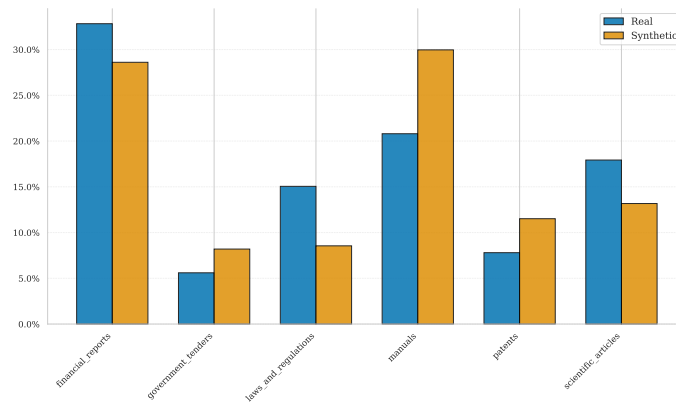
Fig. 23: Comparison between real and synthetic data for DocVQA [38] (a-b) and WTQ [43] (c-d). UMAP embeddings (a, c) show semantic distributions of questions, while bar charts (b, d) compare question type frequencies across datasets.



(a) RVL-CDIP [22]



(b) Tobacco3482 [34]



(c) DocLayNet-CLS [44]

Fig. 24: Comparisons of class distributions between real and synthetic data for RVL-CDIP [22] (a), Tobacco3482 [34] (b) and DocLayNet-CLS [44] (c).



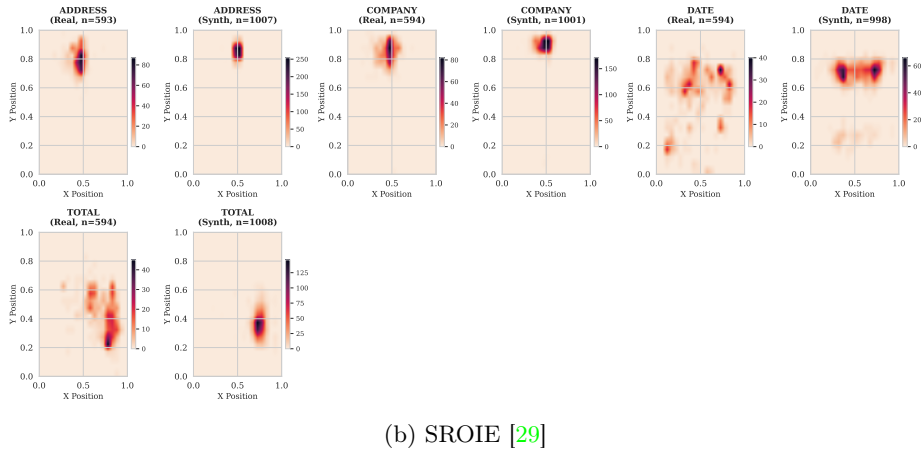
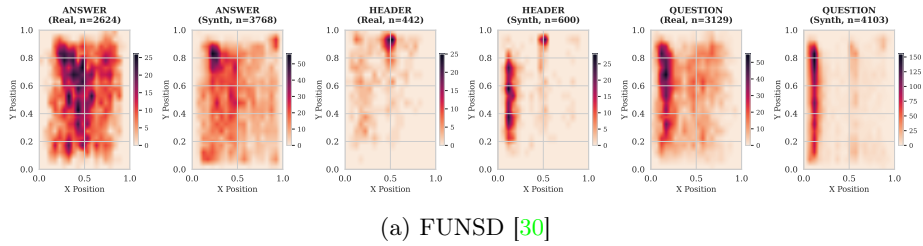


Fig. 26: Heatmaps comparing entity placement by type between real and synthetic data for FUNSD [30] (a) and SROIE [29] (b).

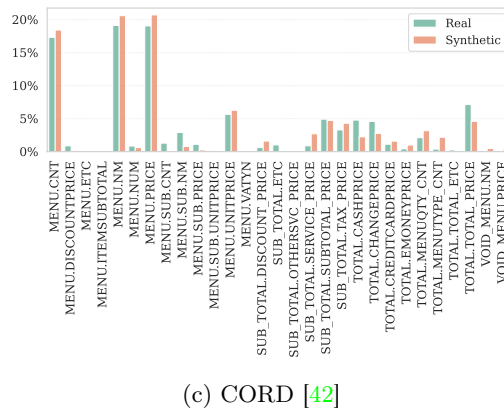
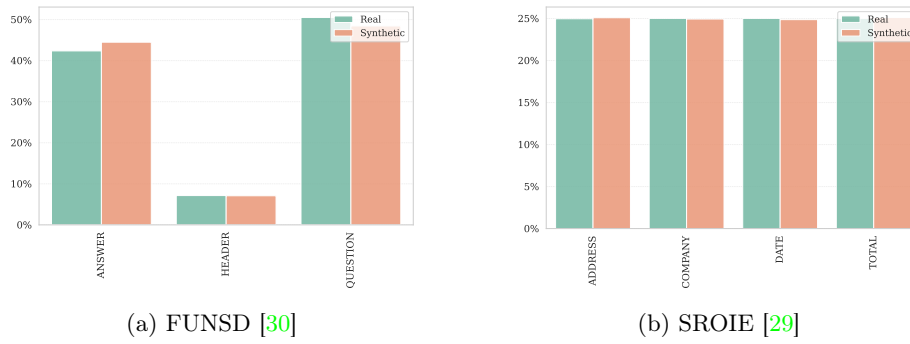


Fig. 27: Comparison of entity type distributions between real and synthetic KIE datasets.

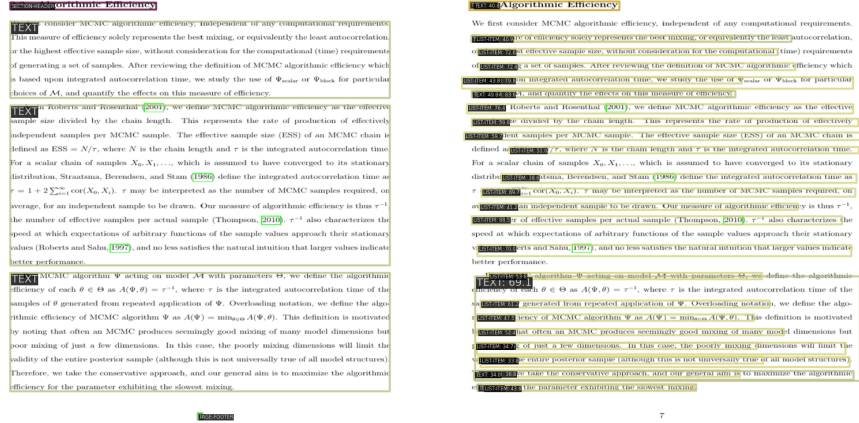


Fig. 28: DocLayNet-DLA [44] GT (left) compared to predictions of Faster R-CNN [49] trained on purely synthetic data (right). Poor performance likely caused by definitional mismatches in list-item classification (distance-based vs. semantic).

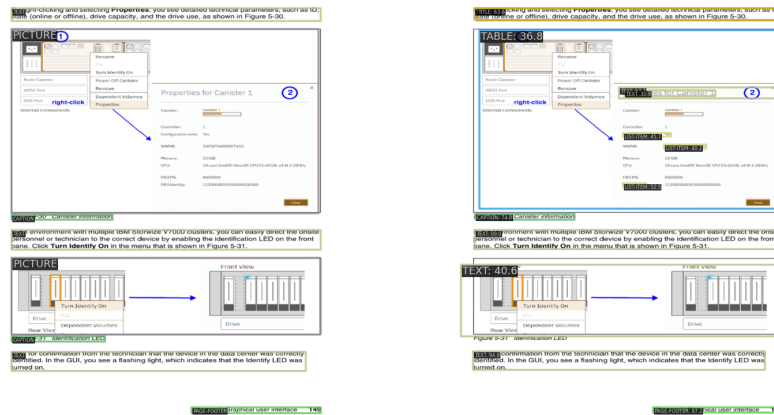


Fig. 29: DocLayNet-DLA [44] GT (left) compared to predictions of Faster R-CNN [49] trained on purely synthetic data (right). Poor performance likely caused by insufficient variety in visual elements to capture complex images with embedded text.

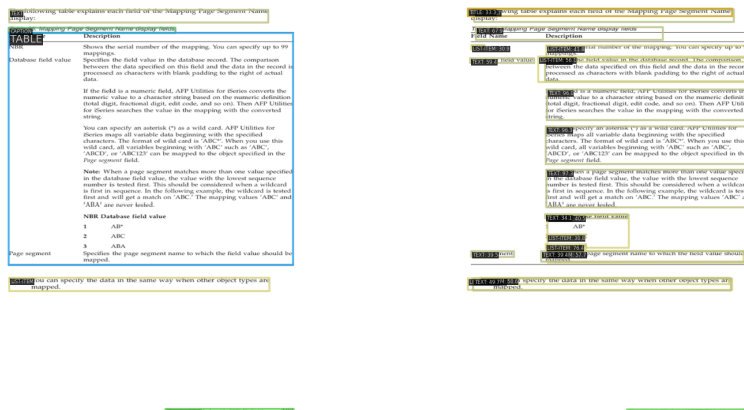


Fig. 30: DocLayNet-DLA [44] GT (left) compared to predictions of Faster R-CNN [49] trained on purely synthetic data (right). Poor performance likely caused by limited table diversity in size and structure in our synthetic data. Our model fails to annotate the region as a single table.

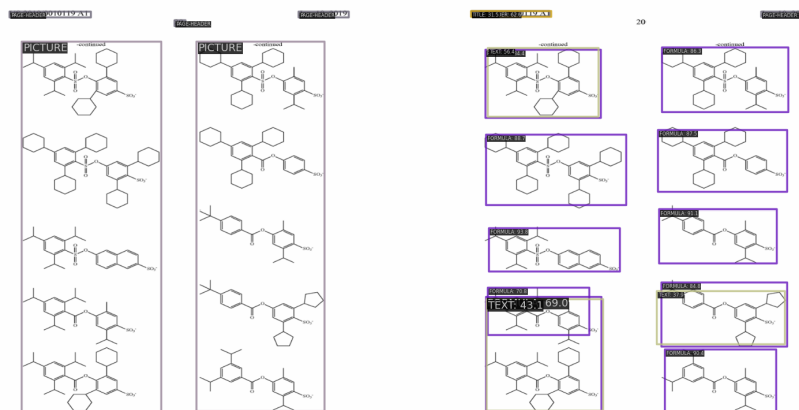
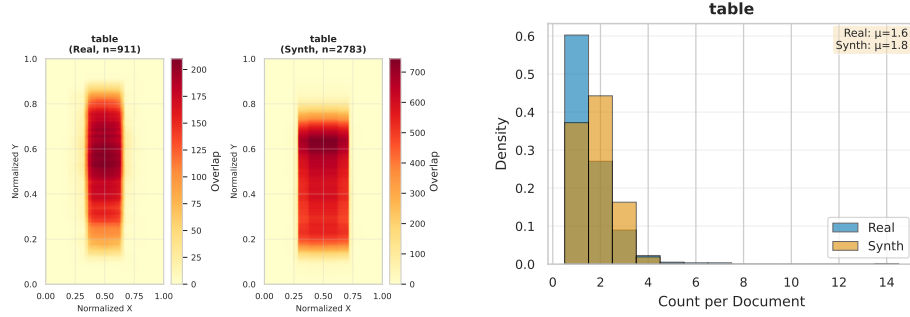
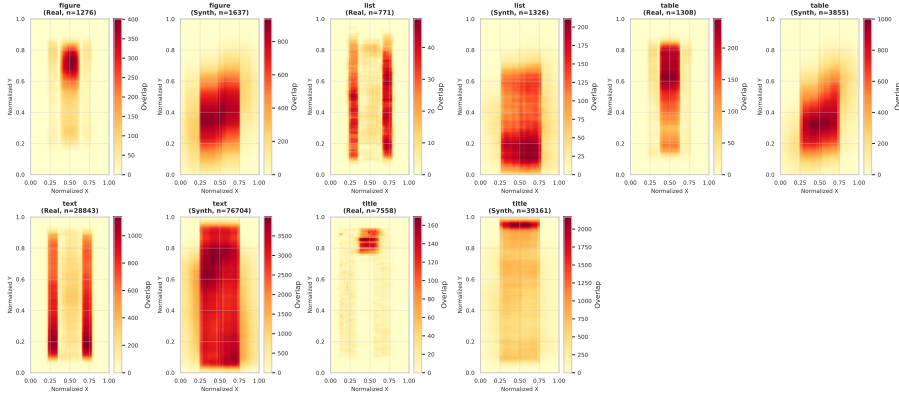


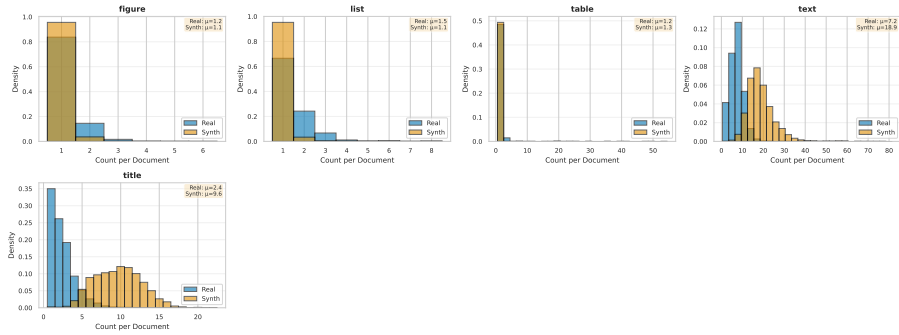
Fig. 31: DocLayNet-DLA [44] GT (left) compared to predictions of Faster R-CNN [49] trained on purely synthetic data (right). Poor performance likely caused by insufficient detailed GT specification. Real GT annotates the formulas as "Picture", while our model annotates them as "Formula".



(a) ICDAR2019 [18] spatial heatmaps. (b) ICDAR2019 [18] region counts.

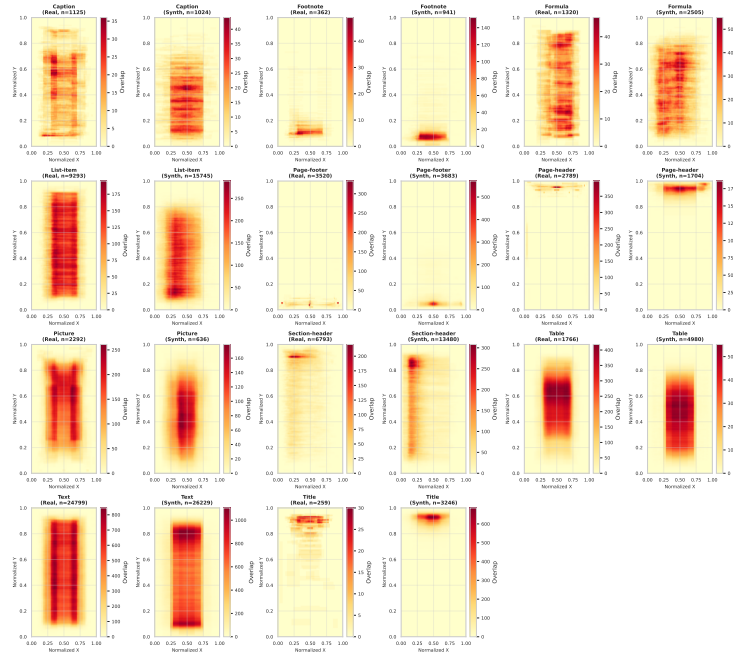


(c) PubLayNet [60] spatial heatmaps.

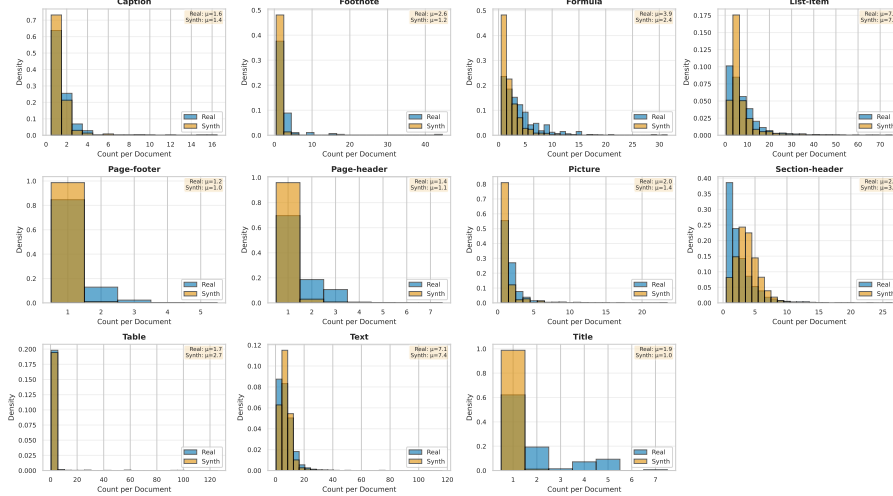


(d) PubLayNet [60] region counts.

Fig. 32: Comparison of annotation spatial heatmaps and class distributions for real and synthetic versions of ICDAR2019 [18] (a, b) and PubLayNet [60] (c, d).



(a) DocLayNet-DLA [44] spatial heatmaps.



(b) DocLayNet-DLA [44] region counts.

Fig. 33: Comparison of annotation spatial heatmaps (top) and class distributions (bottom) for real and synthetic versions of DocLayNet-DLA [44].